Am J Cancer Res 2022;12(5):2050-2067
www.ajcr.us /ISSN:2156-6976/ajcr0141507

Original Article

An immunosuppressive scoring system to predict recurrence and assist in decision regarding postoperative adjuvant treatment in gastric cancer

Jiabin Wang[1,2,3*], Qingzhu Qiu[1,2,3*], Ningzi Lian[1,2,3], Huagen Wang[1,2,3], Qiaoling Zheng[4], Yinghong Yang[4], Yubin Ma[5], Yajun Zhao[6], Ping Li[1,2,3], Jianxian Lin[1,2,3], Jun Lu[1,2,3], Qiyue Chen[1,2,3], Longlong Cao[1,2,3], Mi Lin[1,2,3], Changming Huang[1,2,3], Jianwei Xie[1,2,3]

[1]Department of Gastric Surgery, Fujian Medical University Union Hospital, Fuzhou, Fujian, China; [2]Key Laboratory of Gastrointestinal Cancer (Fujian Medical University), Ministry of Education, Fuzhou, Fujian, China; [3]Fujian Key Laboratory of Tumor Microbiology, Department of Medical Microbiology, Fujian Medical University, Fuzhou, Fujian, China; [4]Department of Pathology, Fujian Medical University Union Hospital, Fuzhou, Fujian, China; [5]Department of Gastrointestinal Surgery, The Affiliated Hospital of Qinghai University, Xining, Qinghai, China; [6]Department of Gastrointestinal Surgery, West District of The First Affiliated Hospital of USTC, Division of Life Sciences and Medicine, University of Science and Technology of China, Hefei, Anhui, China. [*]Equal contributors.

Received January 4, 2022; Accepted April 11, 2022; Epub May 15, 2022; Published May 30, 2022

Abstract: Inhibition of the immune microenvironment is the main cause of tumor recurrence after surgery in patients with gastric cancer (GC). In this study, immunohistochemistry and multiple immunofluorescence staining were used to evaluate immunosuppressive indicators and immune biomarkers in 825 patients with gastric cancer from three centers. We constructed an immunosuppressive recurrence score (IRS) using LASSO Cox regression based on the expression of six immunosuppressive indicators and found that the IRS and IRS-based nomogram were significantly accurate and reliable in predicting recurrence. Moreover, an elevated IRS was associated with locoregional recurrence and postoperative adjuvant chemotherapy failure. Furthermore, an increase in IRS indicated inhibition of the antitumor effect of $CD8^+$ tumor-infiltrating lymphocytes in the invasive margin. Thus, we propose that the IRS can predict the recurrence outcome of patients with GC by distinguishing the immunosuppressive status, which is helpful in the selection of individualized adjuvant treatment plans.

Keywords: Recurrence, immunosuppressive indicators, immune context, adjuvant therapy, gastric cancer

Introduction

Recurrence is the main cause of poor postoperative prognosis of gastric cancer (GC) [1]. Approximately 40-60% of patients with GC will have recurrence postoperatively [2, 3], including local recurrence, peritoneal metastasis, and distant recurrence [4, 5]. Currently, postoperative adjuvant chemotherapy is an important treatment to reduce the risk of recurrence in patients with GC [6, 7]. Chemotherapy can directly kill tumor cells or increase their susceptibility to immune effects to promote tumor-killing activity [8, 9]; however, chemotherapy resistance limits its clinical application. Recently, immunotherapy has shown significant antitumor effects in the treatment of various solid tumors. Immunotherapy has become the first-line treatment for some tumors since it can enhance the antitumor effect of the immune system by reactivating the suppressed immune microenvironment [10-15]. However, immunotherapy does not have a high response rate in GC [16], which may be caused by the heterogeneity of the tumor microenvironment (TME) [17, 18]. For example, patients with tumors that have increased immune cell infiltration can benefit more from immunotherapy [17, 19]. Concomitantly, several scholars hypothesized that different immunosuppressive indicators expressed by tumor cells may affect the status of tumor-infiltrating lymphocytes (TILs), ultimately leading to adverse outcomes, such as local recurrence [20]. Therefore, the immune

status may be the key in deciding the treatment and predicting the recurrence of GC.

Inhibition of the immune microenvironment is an important factor that leads to tumor recurrence. The normal immune system function of the body can recognize and eliminate tumor cells, while suppression of immune function can lead to tumor development and postoperative recurrence, which may be related to tumor immune escape [21-24]. Therefore, inhibition of the tumor immune escape may be the key to tumor treatment. Inhibition of immune checkpoint proteins may reduce the ability of the TME, thus inhibiting the host antitumor immunity [16]. In GC, immunotherapy based on the anti-PD-1/PD-L1 axis has shown significant clinical efficacy [25, 26]. Differences in the expression of immunosuppressive indicators in tumors can be used to predict the prognosis of patients with GC and evaluate the effect of adjuvant therapy; however, the accuracy based on a single molecule is unsatisfactory. Our previous study reported that a scoring system based on multiple immunosuppressive indicators has higher accuracy in predicting the prognosis of patients with GC [27]. First, these immunosuppressive indicators induce immune cells to release inhibitory factors by reprogramming them, which inhibits the activation and downregulation of TIL infiltration and leads to immunosuppression [29-32]. Moreover, they can reduce the sensitivity of tumor cells to cytotoxic T lymphocytes (CTLs) to escape the immune system or bind to inhibitory receptors on the surface of lymphocytes to mediate apoptosis [28, 29]. For example, CEACAM1 downregulates antitumor immunity by inhibiting the immune response of TILs to cancer cells through the TIM-3 signaling pathway [30]. The immunosuppressive indices CD155 and NECTIN2, which are members of the NECTIN-like molecule family, can affect CTL activity through the PVR-TIGIT axis, thus modifying antitumor immunity [31]. However, it is unclear which immunosuppressive indicators are valuable in predicting GC recurrence. We hope to further explore the potential of a scoring system based on immunosuppressive indicators to guide immunotherapy by predicting the recurrent status and patterns.

In this study, we combined the immunosuppression index with the prognosis of patients with GC and established a signature called the immunosuppressive recurrence score (IRS) to categorize patients with different risks of recurrence. We used this as a basis to predict recurrent patterns in patients at different risks of recurrence. We further validated the ability of the IRS to differentiate immune characteristics to determine the potential benefits of adjuvant chemotherapy and immunotherapy. To a certain extent, IRS can guide surgeons in selecting adjunctive treatment for patients with GC, including immunotherapy and chemotherapy, according to the different risks of recurrence. Simultaneously, IRS can help develop follow-up strategies and screening plans for patients to obtain better treatment outcomes.

Materials and methods

Patients and tissue specimens

This study included 825 patients with GC between January 2010 and October 2015. Among these, 627 patients from the Fujian Medical University Union Hospital were divided into the training cohort (n=418, 2010-2013) and internal validation cohort (n=209, 2013-2015) according to the time of surgery. A total of 198 patients from Qinghai University Hospital (n=110) and the First Affiliated Hospital of the University of Science and Technology of China (n=88) were included in the external validation cohort. The detailed inclusion and exclusion criteria are described in the Supplementary Methods section. The study was approved by the Ethics Committees of Fujian Medical University Union Hospital, the Affiliated Hospital of Qinghai University, and the First Affiliated Hospital of the University of Science and Technology of China. The ethics approval number of the scientific research project was 2021KY018 from the Fujian Medical University Union Hospital. Written informed consent was obtained from all patients before specimen collection.

Definition and classification of recurrence

Recurrence was defined as the presence of a tumor showing GC cells confirmed on tissue biopsy or presence of imaging features that are highly indicative of tumor recurrence. Recurrence was categorized as locoregional, peritoneal implantation, or distant metastasis. Locoregional recurrence included recurrence

in the gastric bed, anastomoses, and perigastric lymph nodes. Recurrence in the duodenum was also defined as local recurrence, belonging to the "others" category in this study.

Immunohistochemistry

Seven immunosuppressive indicators were based on previous immunohistochemistry analysis: SIGLEC6, CD44, CEACAM1, CD155, HMGB1, NECTIN2, and ADENOSINE [32]. The scoring criteria for immunosuppressive indicators were as follows: in five randomly selected fields, the average percentage and intensity of positive cells were evaluated to determine protein expression levels. The scoring criteria (Figure S1) were as follows: the staining intensity was categorized as 0 (no staining), 1 (weak staining, light yellow), 2 (medium staining, yellow to brown), or 3 (strong staining, brown), and the proportion of positive tumor cells was categorized as 0 (≤5% positive cells), 1 (6%-25%), 2 (26%-50%), and 3 (≥51%). The staining intensity score was multiplied by the proportional staining score (total score, 0-9) to calculate the final expression score. Patients with a final score <4 were included in the low-expression group, and those with a score ≥4 were included in the high-expression group.

To assess the immune context of patients with GC, we analyzed total immune cells (CD45), T lymphocytes (CD3), cytotoxic T lymphocytes (CD8), and activated and memory T lymphocytes. To evaluate the infiltration of immune cells, five representative and independent fields at 200 × magnification were captured at the center of tumor (CT) and invasive margin (IM) of each tissue. An example of this procedure is shown in Figure S2. Then, we used the "measurement" plug-in of the Image Pro Plus software (version 6.0; Inc., USA) to assist in marker counting to determine the number of positive cells in the field. The average number of positive cells in the five fields was divided by the area of the field to obtain the infiltration density of immune cells in the CT and IM.

To determine the microsatellite instability (MSI) and Epstein-Barr virus (EBV) status of the patients, MLH1, MSH2, MSH6, and PMS2 immunohistochemical staining and EBER (ISH-6021; ZSGB-BIO) in situ hybridization were performed. The evaluation criteria for MSI and EBV status are shown in Figure S3 and Supplementary Methods.

Two experienced pathologists, blinded to the clinicopathological characteristics and prognosis of the patients, independently scored all samples. When scoring immune checkpoints and evaluating MSI and EBV status, approximately 93% of the scores were completely concordant. When the scores of the two independent pathologists varied, another pathologist reviewed the results and selected one of the scores of the first two pathologists or the three pathologists arrived at a consensus. Details of the antibodies used in this study are presented in Table S1.

Building the IRS using the LASSO Cox regression model

The least absolute shrinkage and selection operator (LASSO) Cox regression model was used to integrate seven significant indicators and eliminate the offset caused by the correlation between variables to build a signature for predicting recurrence in the training cohort (n=418). We use the "glmnet" package of R software (version 4.0.0) to analyze the data using the LASSO Cox regression model. The three risk groups were distinguished according to the optimal cutoff value of the IRS using X-tile software (version 3.6.1).

Multiplexed immunofluorescence staining and analysis

To determine the differences in the TME in different IRS risk groups, we performed multiplexed immunofluorescence staining to identify the expression of CD8, PD-1, and TIM-3 using the Opal kit (Perkin-Elmer, USA) in 45 GC tissue samples. In the three risk subgroups of the internal validation cohort, each patient with GC was assigned a random number in each subgroup, and the top 15 patients (ranked from small to large) in each group were selected by a random number, for a total of 45 cases.

We used the Mantra System (PerkinElmer, USA) to scan the multiplexed immunofluorescence-stained tissues at 200 × magnification and InForm image analysis software (PerkinElmer, USA) to quantify positive cells automatically. To ensure the accuracy of the results, two pathologists individually verified the results using the

aforementioned method. When the difference between the software results and those of the two pathologists was within 5%, the average of the two results was obtained. If the difference exceeded 5%, the two pathologists reassessed the results and a third pathologist was asked to evaluate the results. Finally, the third pathologist decided which result would be accepted. The detailed steps are shown in Supplementary Methods.

Statistical analysis

SPSS (version 26.0, IBM, Inc., USA) and R software (version 4.0.0) were used to process all data. The Mann-Whitney U test was used to compare the two groups, and the Kruskal-Wallis test to perform multiple comparisons. Categorical variables of clinicopathological characteristics were compared using χ^2 test or Fisher's exact test. Nonparametric correlation analyses were performed using the Spearman's test. Kaplan-Meier survival analysis with log-rank test was used to estimate recurrence-free survival (RFS). The Cox proportional hazard model was used to confirm the association between the relevant clinicopathological variables and RFS. Significant variables after the univariate Cox analysis were included in the multivariate Cox analysis. Statistical significance was set at *P*-value <0.05.

Results

Patient characteristics and construction of the IRS

The clinicopathological data of 825 patients with GC are presented in **Table 1**, and a flow chart of this study is shown in **Figure 1**.

To verify the prognostic value of immunosuppressive indicators (SIGLEC6, CD44, CEACAM1, CD155, HMGB1, NECTIN2, and ADENOSINE) for RFS, immunohistochemistry was performed to evaluate the expression of these seven indicators in GC specimens from 825 patients in three centers (**Figure 2A**). As hypothesized, patients with GC with low expression of all seven indicators showed lower recurrence rates (Figure S4A-C). Our previous study reported a correlation between the seven immunosuppressive indicators [27]. To reduce the impact of correlations between these seven indicators and construct a scoring system, we used the LASSO Cox regression model to fit the RFS data from the training cohort. In the optimization model, six of the seven indicators were selected, and the six selected indicators and their corresponding regression coefficients (**Figure 2B** and **2C**) were used to derive the model formula. The following formula was used to calculate the IRS for each patient: IRS=0.17543 × CEACAM1 + 0.04265 × SIGLEC6 + 0.20185 × CD44 + 0.05687 × CD155 + 0.02017 × ADENOSINE - 0.0507 × NECTIN2. In the formula generated by the LASSO Cox regression model, the HMGB1 indicator was excluded, which was attributed to the correlation coefficient of 0 (less critical in the formula). To explore the clinical characteristics of patients with GC with different IRS scores, we divided these patients into three subgroups (low risk, 0-1.92; moderate risk, 1.93-3.02; and high risk, 3.03-5) according to the cutoff point calculated using X-tile software (Figure S5A-C). As mentioned above, we classified patients with GC into three subgroups according to the IRS that we constructed based on six immunosuppressive signatures. This provided the basis for our analysis of the clinical outcomes and immune cell infiltration.

Value of IRS in predicting recurrence

Receiver operating characteristic (ROC) curve analysis displayed that the IRS could accurately predict the outcome of recurrence in different years (**Figure 3A-C**). The three risk subgroups showed significant differences in the five-year recurrence rate (**Figure 3D-F**). Similar results were obtained in patients with different clinicopathological factors (except for those in stage I) (Figures S6, S7, S8). The χ^2 test was performed in the three cohorts to compare the differences in clinicopathological variables in different risk groups, and there was no significant difference except for TNM stage and CA19-9 level (Tables S2, S3). Univariate and multivariate analyses using the Cox regression model showed that IRS was a powerful and independent factor for RFS (Tables S4, S5, S6). The abovementioned results revealed that IRS is a powerful and independent factor and could significantly distinguish postoperative patients with GC with different risks of recurrence.

IRS was correlated with postoperative recurrence time

We analyzed the composition of patients with different clinical outcomes among the three

Table 1. Clinicopathological characteristics of the patients with GC in each cohort

Variable	Internal Cohort				External	
	Training Cohort		Validation Cohort		Validation Cohort	
	N	%	N	%	N	%
Total patients	418	-	209	-	198	-
Age (years)						
≤65	246	58.9	120	57.4	140	70.7
>65	172	41.1	89	42.6	58	29.3
Sex						
Female	98	23.4	57	27.3	60	30.3
Male	320	76.7	152	72.7	138	69.7
BMI						
≤25	351	84.0	178	85.2	-	-
>25	67	16.0	31	14.8	-	-
Resection type						
Partial gastrectomy	183	43.8	97	46.4	144	72.7
Total gastrectomy	235	56.2	112	53.6	54	27.3
Tumor size						
≤50 mm	230	55.0	112	53.6	137	69.2
>50 mm	188	45.0	97	46.4	61	30.8
Tumor location						
Cardia	101	24.2	52	24.9	-	-
Body	88	21.1	32	15.3	-	-
Antrum	186	44.6	93	44.5	-	-
Whole	43	10.1	32	15.3	-	-
Grade						
Low	189	45.2	105	50.2	67	33.8
Moderate + High	144	34.5	68	32.6	76	38.4
Mix	67	16.0	33	15.8	52	26.3
Unknown	18	4.3	3	1.4	3	1.5
Depth of invasion						
T1	37	8.8	36	17.2	36	18.2
T2	47	11.2	22	10.5	41	20.7
T3	151	36.1	92	44.0	17	8.6
T4	183	43.8	59	28.2	104	52.5
Lymph node metastasis						
N0	94	22.5	71	34.0	94	47.5
N1	76	18.2	40	19.1	34	17.1
N2	88	21.0	32	15.3	31	15.7
N3	160	38.3	66	31.6	39	19.7
AJCC (7th)						
I	55	13.2	44	21.1	57	28.8
II	113	27.0	64	30.6	53	26.8
III	250	59.8	101	48.3	88	44.4
MSI status						
MSS/MSI-L	337	80.6	169	80.9	144	72.7
MSI-H	81	19.4	40	19.1	54	27.3
EBV status						
Negative	393	94.0	196	93.8	189	95.5
Positive	25	6.0	13	6.2	9	4.5

Adjuvant chemotherapy						
Yes	221	52.9	110	52.6	100	50.5
No	197	47.1	99	47.4	98	49.5
CEA						
Normal	346	82.8	191	91.4	-	-
Elevated	72	17.2	18	8.6	-	-
CA19-9						
Normal	330	78.9	166	79.4	-	-
Elevated	88	21.1	43	20.6	-	-

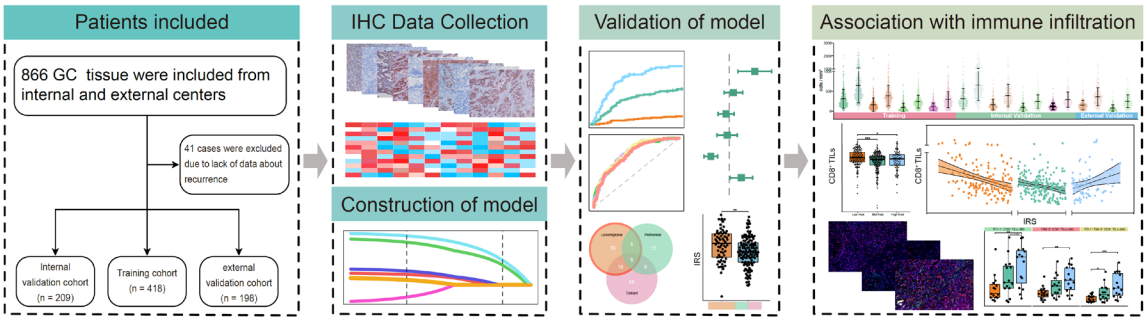

Figure 1. Workflow of the study.

groups. In the high-risk group, 45.2% of the total group had recurrence within 1 year, while the percentage was only 2.7% in the low-risk group and between the values of the other two groups in the moderate-risk group. The results were also applicable to patients with recurrence within 2 and 3 years, but the opposite was observed in patients without recurrence (P<0.001, **Figure 3G-I**). The significant difference in recurrence status among the three risk groups led us to hypothesize that the IRS score was related to RFS. As expected, patients with early recurrence had higher IRS scores than those with late recurrence (**Figure 3J**). We obtained similar results in the internal and external cohorts (**Figure 3K** and **3L**), and insufficient number of patients with recurrence after 5 years in the external cohort did not affect our conclusions. In summary, patients with GC with higher IRS scores were more likely to have relapse within a shorter time after surgery.

IRS predicts the benefit of chemotherapy

As shown in Figure S9, chemotherapy significantly reduced the recurrence rate in the moderate-risk group, whereas in the high-risk group, patients failed to benefit from chemotherapy. In the low-risk group, the overall recurrence rate was low, and chemotherapy did not improve the recurrence rate. The results were consistent between the training cohort and the internal and external validation cohorts.

IRS predicts recurrence patterns

The recurrence patterns in the training and internal validation cohorts are shown in **Figure 4A**. To explore whether IRS can predict recurrence patterns, we compared the IRS of patients with and without locoregional recurrence among all patients who had recurrence. **Figure 4B** and **4C** shows that patients with locoregional recurrence had significantly higher IRS scores (P=0.002). However, patients with peritoneal and distant metastases did not show any diversity (Figure S10A and S10B). We also found that patients with locoregional recurrence (Figure S10C) showed different recurrence sites and patients with recurrence of perigastric lymph nodes had a higher IRS than patients without recurrence of lymph nodes (P=0.034, **Figure 4D**).

IRS is related to the infiltration of T lymphocytes in the IM

To explore the reason that patients with higher IRS relapsed earlier and more easily and had higher risk of locoregional recurrence (espe-

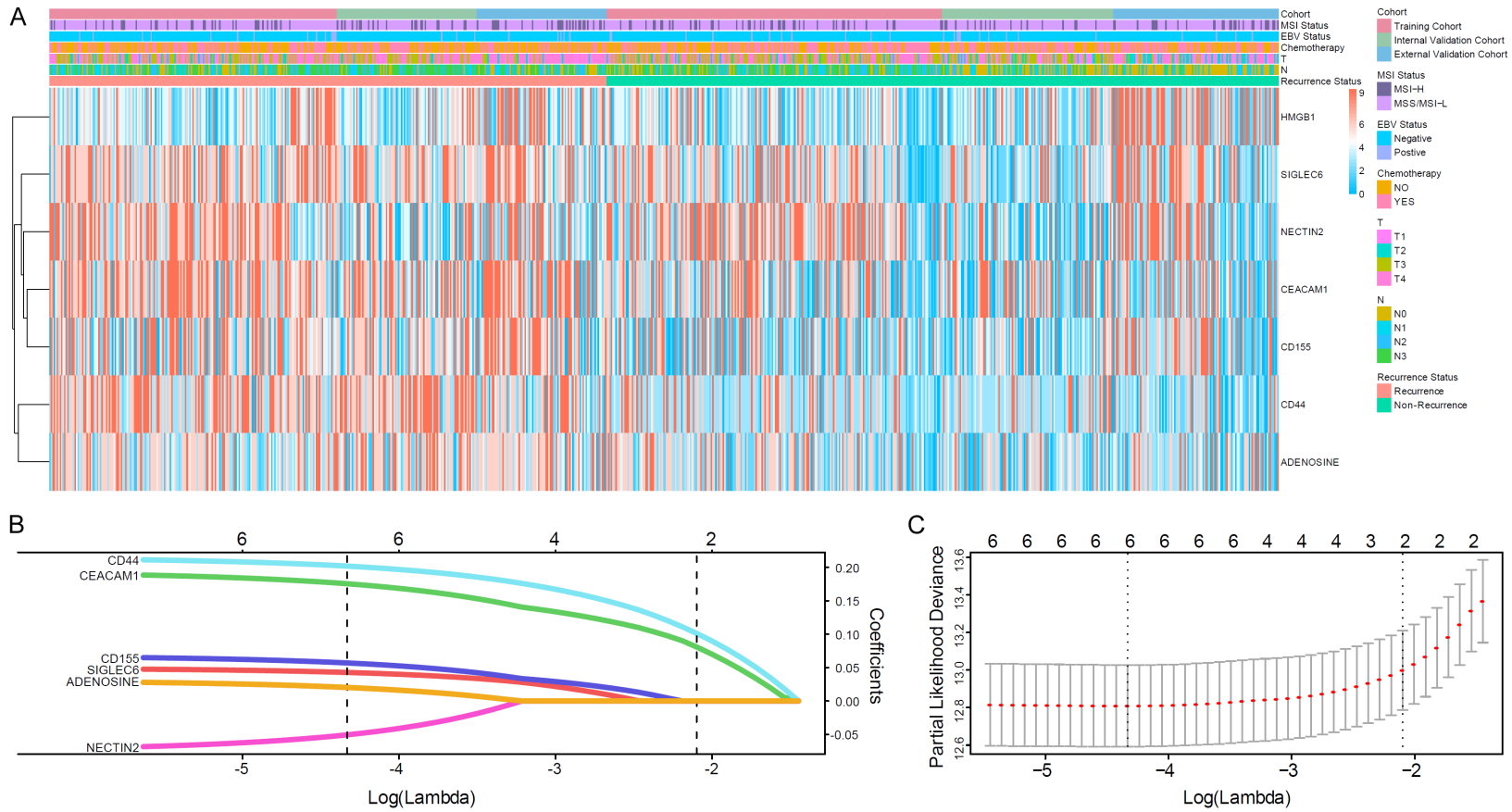

Figure 2. Construction of the immunosuppressive recurrence score (IRS) using the LASSO Cox regression model. A. Heatmap showing the immunohistochemistry scores of seven immunosuppressive checkpoints (HMGB1, SIGLEC6, NECTIN2, CEACAM1, CD155, CD44, and ADENOSINE) in the training cohort (*n*=418), internal validation cohort (*n*=209), and external validation cohort (*n*=198). B. Construction of the IRS using the LASSO Cox regression method; the LASSO coefficient of the six immunosuppressive checkpoints is shown. C. The tenfold cross-validation of fine-tuning parameter selection in the LASSO model.

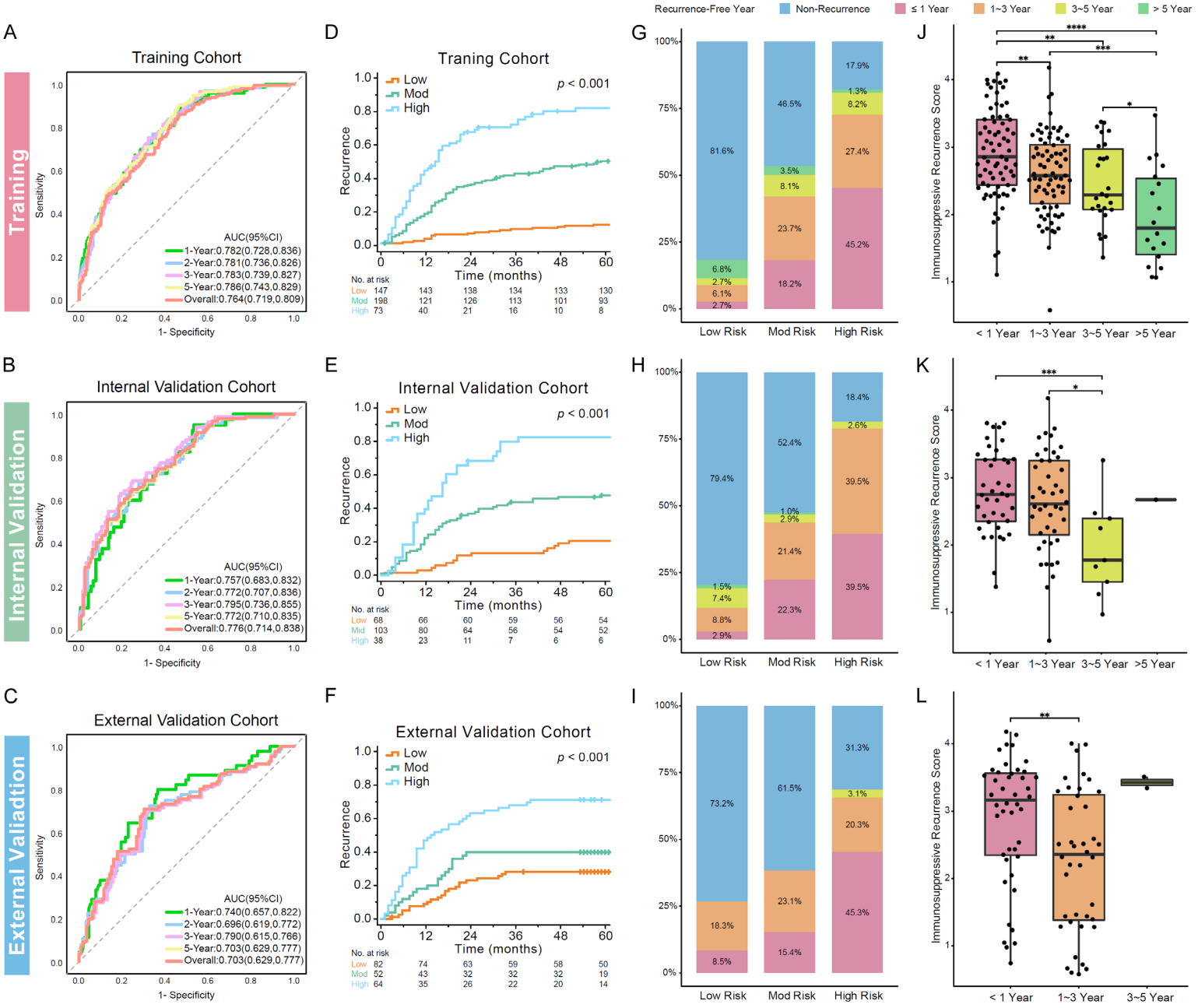
A
Training Cohort
Training
Sensitivity
1- Specificity
AUC(95%CI)
1-Year:0.782(0.728,0.836)
2-Year:0.781(0.736,0.826)
3-Year:0.783(0.739,0.827)
5-Year:0.786(0.743,0.829)
Overall:0.764(0.719,0.809)
B
Internal Validation Cohort
Internal Validation
AUC(95%CI)
1-Year:0.757(0.683,0.832)
2-Year:0.772(0.707,0.836)
3-Year:0.795(0.736,0.855)
5-Year:0.772(0.710,0.835)
Overall:0.776(0.714,0.838)
C
External Validation Cohort
External Valiadtion
AUC(95%CI)
1-Year:0.740(0.657,0.822)
2-Year:0.696(0.619,0.772)
3-Year:0.790(0.615,0.766)
5-Year:0.703(0.629,0.777)
Overall:0.703(0.629,0.777)
D
Traning Cohort
Low
Mod
High
p < 0.001
Recurrence
Time (months)
No. at risk
Low 147 143 138 134 133 130
Mod 198 121 126 113 101 93
High 73 40 21 16 10 8
E
Internal Validation Cohort
Low
Mod
High
p < 0.001
Recurrence
Time (months)
No. at risk
Low 68 66 60 59 56 54
Mid 103 80 64 56 54 52
High 38 23 11 7 6 6
F
External Validation Cohort
Low
Mod
High
p < 0.001
Recurrence
Time (months)
No. at risk
Low 82 74 63 59 58 50
Mod 52 43 32 32 32 19
High 64 35 26 22 20 14
G
Recurrence-Free Year
Non-Recurrence
≤ 1 Year
1~3 Year
3~5 Year
> 5 Year
81.6%
6.8%
2.7%
6.1%
2.7%
46.5%
3.5%
8.1%
23.7%
18.2%
17.9%
1.3%
8.2%
27.4%
45.2%
Low Risk
Mod Risk
High Risk
H
79.4%
1.5%
7.4%
8.8%
2.9%
52.4%
1.0%
2.9%
21.4%
22.3%
18.4%
2.6%
39.5%
39.5%
Low Risk
Mod Risk
High Risk
I
73.2%
18.3%
8.5%
61.5%
23.1%
15.4%
31.3%
3.1%
20.3%
45.3%
Low Risk
Mod Risk
High Risk
J
Immunosuppressive Recurrence Score
< 1 Year
1~3 Year
3~5 Year
>5 Year
K
Immunosuppressive Recurrence Score
< 1 Year
1~3 Year
3~5 Year
>5 Year
L
Immunosuppressive Recurrence Score
< 1 Year
1~3 Year
3~5 Year

Figure 3. Data from three independent cohorts point out that IRS remarkably predicts recurrence in gastric cancer. A-C. Time-dependent receiver operator characteristic (ROC) curves of IRS for recurrence-free survival (RFS) in the training (n=418), internal validation (n=209), and external validation (n=198) cohorts. D-F. Kaplan-Meier curves for RFS according to IRS in the training, internal validation, and external validation cohorts. G-I. Compositions of recurrence status and recurrence time in the low-, moderate-, and high-risk groups in the training, internal validation, and external validation cohorts. P<0.001, P<0.001, P=0.007, respectively (Fisher's exact test). J-L. Comparison of IRS between patients with gastric cancer (GC) with different recurrence times in the training, internal validation, and external validation cohorts. *P<0.05; **P<0.01; ***P<0.001; ****P<0.0001; non-significant values are shown as blanks (Kruskal-Wallis test).

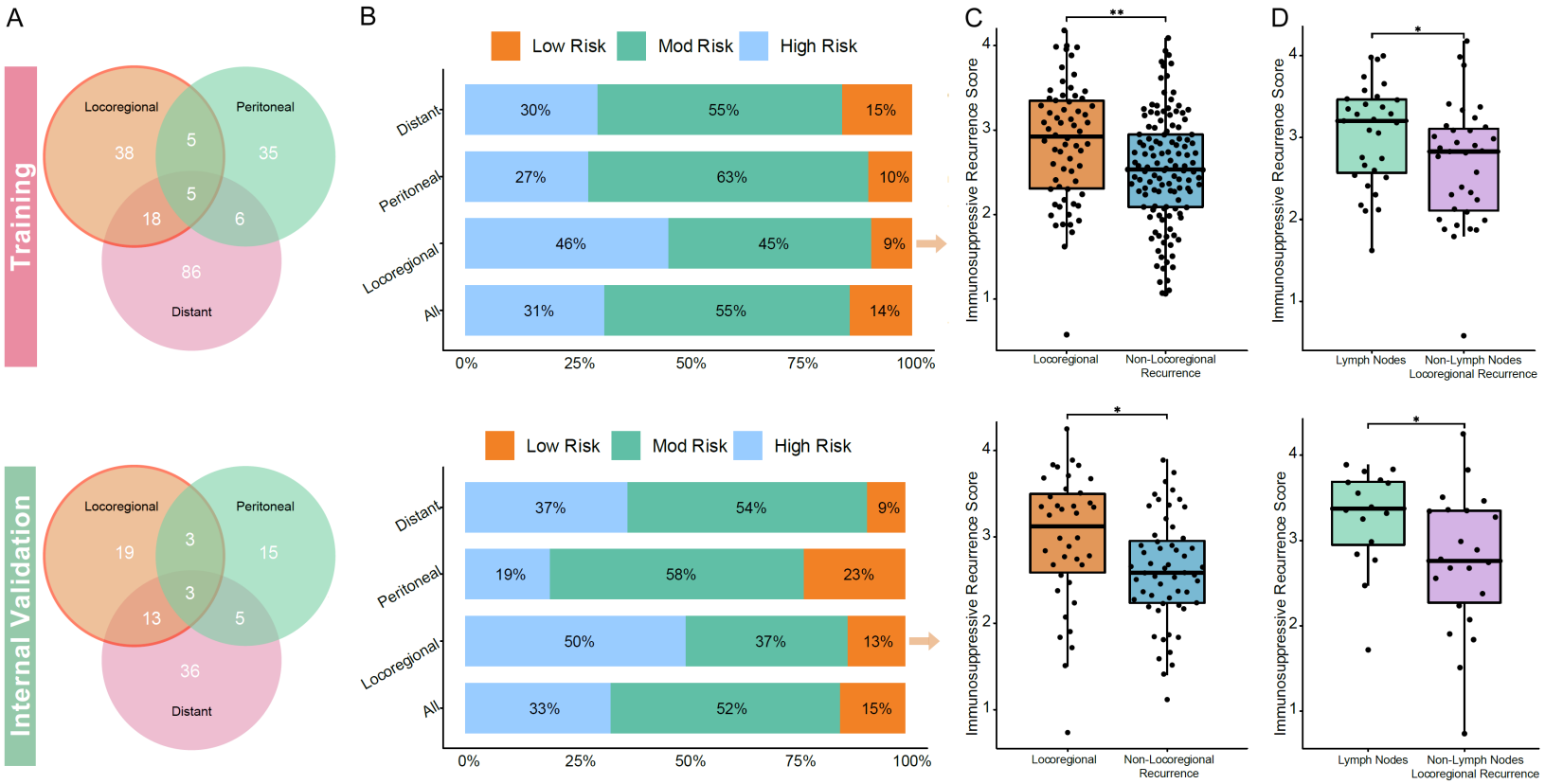

Figure 4. Locoregional recurrence, especially in the perigastric lymph nodes, tends to occur in patients with GC with higher IRS. A. Venn diagram of recurrence patterns in the internal cohorts with documented recurrence. B. Proportions of three subgroups (low-, moderate-, and high-risk subgroups) of patients with different recurrence patterns in the internal cohorts. C. Comparison of IRS between patients with locoregional recurrence and patients with non-locoregional recurrence in the internal cohorts. D. Among all patients with gastric cancer (GC) with locoregional recurrence, IRS was compared between patients with recurrence in lymph node and patients with non-lymph node locoregional recurrence in the internal cohorts. *P<0.05; **P<0.01 (Mann-Whitney U test).

cially in the perigastric lymph node area), we investigated the correlation between IRS and immune cell infiltration. Immune cell quantification revealed a large difference in immune cell infiltration between the CT and IM; therefore, these two areas were analyzed separately (**Figure 5A**).

First, we evaluated leukocyte infiltration ($CD45^+$). However, in patients with different recurrence outcomes, there was no significant difference in leukocyte infiltration, in either the IM or CT (**Figures 5B**, S11, S12). Subsequently, we narrowed the scope of our study to TILs. The densities of $CD3^+_{(IM)}$ and $CD8^+_{(IM)}$ TILs were negatively correlated with IRS in the low- and moderate-risk groups, but a reverse trend was observed in the high-risk group (**Figure 5B-D**). The highest $CD3^+_{(IM)}$ and $CD8^+_{(IM)}$ TIL levels were found in the low-risk group (**Figures 5E**, **5F**, S12, S13). However, this difference was not observed in memory T ($CD45RO^+$) cells (**Figures 5B**, S11, S12).

Increased IRS indicated suppression of the effect of $CD8^+_{(IM)}$ T lymphocytes

As the executors of killing tumor cells, $CD8^+$ TILs have been associated with better prognostic outcomes in many studies [33-35]. However, abundant $CD8^+$ lymphocytes were present in the high-risk (worst prognosis) group of patients with GC, which evoked our interest. We hypothesized that $CD8^+$ TILs may have poor antitumor effects in the high-risk group of patients with GC. The co-positivity of PD-1 and TIM-3 in T lymphocytes represents a hypofunctional host environment [36-38]. Therefore, we performed a multiplexed immunofluorescence analysis of 45 GC specimens to investigate the expression of PD-1 and TIM-3 in all subgroups (Table S7). **Figure 6A** shows the expression of PD-1 and TIM-3 in $CD8^+_{(IM)}$ T lymphocytes in the low-, moderate-, and high-risk groups. Approximately 28.8% and 18.8% of $CD8^+$ lymphocytes in the IM expressed PD-1 and TIM-3, respectively, and 12.1% co-expressed those (**Figure 6B** and **6C**). In the high-risk group, $PD\text{-}1^+CD8^+_{(IM)}$ and $PD\text{-}1^+TIM\text{-}3^+CD8^+_{(IM)}$ T lymphocytes displayed higher densities than those in the low- and moderate-risk groups (**Figure 6D**). The proportion of $CD8^+_{(IM)}$ TILs expressing these two inhibitory receptors in the three subgroups was also diverse. $CD8^+_{(IM)}$ T lymphocytes showed the highest proportion of PD-1 or TIM-3 expression or a combination of the two in the high-risk group (**Figure 6E**). For $CD8^+_{(CT)}$ T lymphocytes, no significant difference was observed (Figure S14).

Building a nomogram based on IRS to predict recurrence

To facilitate the clinical application of IRS to predict recurrence in individual patients, we built a nomogram (**Figure 7A**) based on the Cox regression model and integrated IRS and clinicopathological factors (T stage, N stage, adjuvant chemotherapy, and CA19-9 level). ROC analysis showed that the nomogram had a high accuracy in predicting 1-, 3-, and 5-year recurrences. Calibration analysis verified the reliability of the nomogram, and the decision curve analysis (DCA) showed its clinical usefulness (**Figures 7B-D**, S15). For patients who underwent GC resection, the IRS-based nomogram had better reliability, accuracy, and clinical availability in predicting recurrence. Furthermore, it was stable in predicting recurrence in different time periods.

Discussion

In this study, we constructed a simple and reliable IRS based on six immunosuppressive indicators expressed in GC tissues to characterize the immune microenvironment of GC and predict the RFS and pattern of recurrence. The results showed that patients with GC with an elevated IRS may be at high risk for early and locoregional recurrence. Moreover, IRS was able to identify patients with GC who responded to adjuvant chemotherapy. Our results suggest that postoperative adjuvant chemotherapy is essential in reducing the risk of recurrence in patients with moderate risk. We also provide an example of the potential application of IRS, where an IRS-based nomogram demonstrated strong recurrence prognostic value and was validated in three independent cohorts. In summary, we believe that the IRS has important clinical application potential in predicting recurrence in individual patients.

Inhibition of the immune microenvironment is a marker of GC progression and plays a crucial role in tumor recurrence [39, 40]. In addition to PD-L1, other immunosuppressive molecules are thought to act alone or in combination with

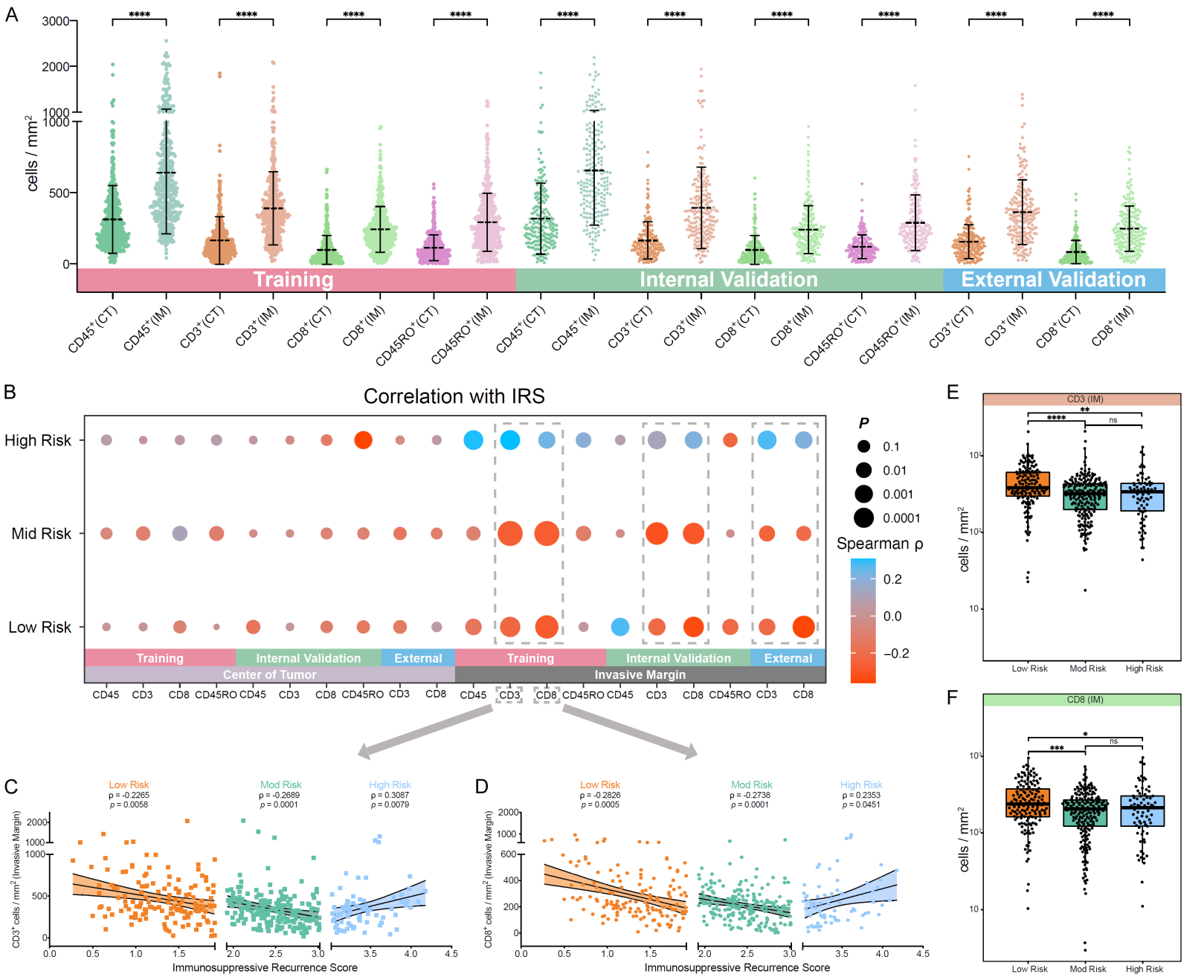
A
cells / mm²
Training
Internal Validation
External Validation
CD45⁺(CT)
CD45⁺(IM)
CD3⁺(CT)
CD3⁺(IM)
CD8⁺(CT)
CD8⁺(IM)
CD45RO⁺(CT)
CD45RO⁺(IM)
B
Correlation with IRS
High Risk
Mid Risk
Low Risk
Training
Internal Validation
External
Center of Tumor
Invasive Margin
P
Spearman ρ
C
Low Risk
Mod Risk
High Risk
Immunosuppressive Recurrence Score
D
Immunosuppressive Recurrence Score
E
CD3 (IM)
F
CD8 (IM)

Figure 5. IRS correlated with $CD3^+$ and $CD8^+$ TIL infiltration in the invasive margin (IM). A. Expression of four immune biomarkers ($CD45^+$, $CD3^+$, $CD8^+$, $CD45RO^+$) in the center of the tumor (CT) and invasive margin (IM) of patients with GC from the internal cohorts (*n*=627), and the expression of two immune biomarkers ($CD3^+$, $CD8^+$) in the CT and IM of patients with GC from the external validation cohort (*n*=198). ****P<0.0001 (paired t-test). Error bar indicates mean and standard deviation. B. Correlation between IRS values and infiltration levels of immune biomarkers (CT and IM) in the training, internal validation, and external validation cohorts (Spearman correlation test). C, D. Correlation between IRS values and infiltration levels of $CD3^+_{(IM)}$ and $CD8^+_{(IM)}$ in the training cohort of patients with GC (Spearman correlation test). E, F. Comparison of the expression of $CD3^+_{(IM)}$ and $CD8^+_{(IM)}$ in three subgroups (low-, moderate-, and high-risk subgroups) of patients with GC from the training cohort. *P<0.05; **P<0.01; ****P<0.0001; ns, not significant (Kruskal-Wallis test).

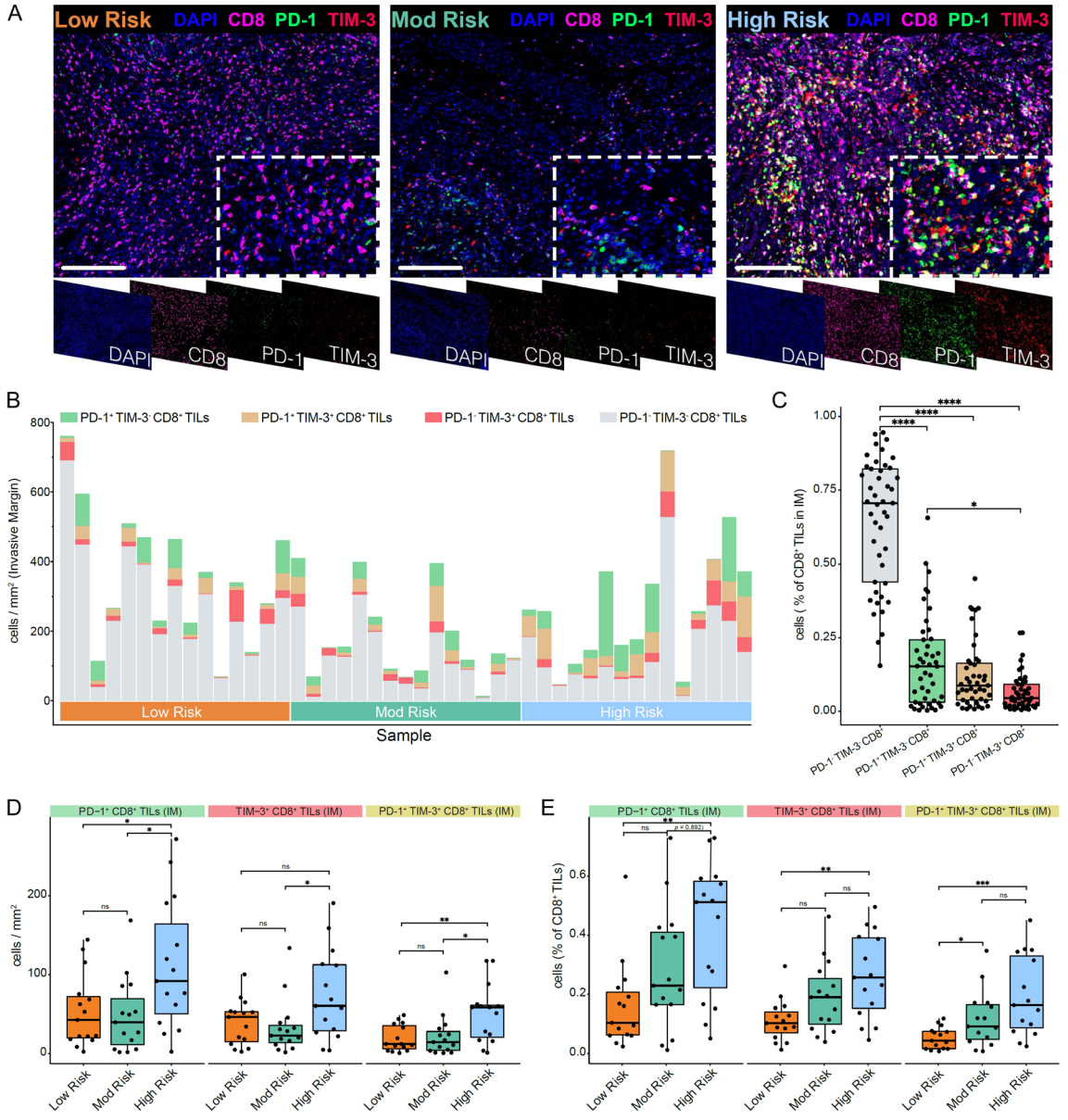

Figure 6. Multiplexed immunofluorescence (IF) staining reveals that the expression of immune checkpoints (PD-1 and TIM-3) was upregulated in the invasive margin (IM) in the high-risk group. A. Representative multiplexed IF images showing the expression of PD-1 and TIM-3 in $CD8^+$ lymphocytes in the three risk subgroups of patients with GC. B. In the low- (*n*=15), moderate- (*n*=15), and high-risk (*n*=15) groups, the different subtypes of $CD8^+$ lymphocytes were classified according to PD-1 and TIM-3 expression. C. Percentages of $PD\text{-}1^-TIM\text{-}3^-CD8^+_{(IM)}$, $PD\text{-}1^+TIM\text{-}3^-CD8^+_{(IM)}$, $PD\text{-}1^+TIM\text{-}3^+CD8^+_{(IM)}$, and $PD\text{-}1^-TIM^+CD8^+_{(IM)}$ T lymphocytes in 45 patients with GC. D. Comparison of the expression of $PD\text{-}1^+CD8^+_{(IM)}$, $TIM\text{-}3^+CD8^+_{(IM)}$, and $PD\text{-}1^+TIM\text{-}3^+CD8^+_{(IM)}$ in the low-risk (*n*=15), moderate-risk (*n*=15), and high-

risk (n=15) risk groups of patients with GC. E. Comparison of the percentages of $CD8^+$ lymphocytes expressing $PD\text{-}1^+CD8^+_{(IM)}$, $TIM\text{-}3^+CD8^+_{(IM)}$, and $PD\text{-}1^+TIM\text{-}3^+CD8^+_{(IM)}$ in the low-risk (n=15), moderate-risk (n=15), and high-risk (n=15) groups of patients with GC. *P<0.05; **P<0.01; ***P<0.001; ****P<0.0001; ns, not significant (Kruskal-Wallis test). Scale bar =200 μm.

PD-L1 to downregulate antitumor immunity. They promote immunosuppression by reducing TIL infiltration, inhibiting T cell activation, recruiting inhibitory cells (e.g., regulatory T cells or myeloid inhibitory cells), or increasing the expression of inhibitory receptors [28, 39, 41-45]. Based on the results of previous studies, we identified seven immunosuppressive indices that are significant for GC recurrence [27]. We used LASSO Cox regression analysis to eliminate the correlation between indicators. Finally, we excluded HMGB1 from the formula because the predictive effect of HMGB1 on GC recurrence could be replaced by other indicators. Our study shows that IRS is a strong and independent factor that can accurately determine the risk of recurrence in patients with GC after surgery. Moreover, the value of IRS in predicting GC recurrence may not be affected by TNM staging, MSI, or EBV status, providing IRS with a wide application value in predicting GC recurrence. Compared to many complex variables required in oncology, IRS-based nomograms can further improve their ability to predict individual patient outcomes and demonstrate significant discrimination, accuracy, and clinical utility, which only requires few immunosuppressive indicators and common clinicopathological information.

There is increasing evidence that TILs, which represent the local immune response [46-48], are associated with the recurrence of several cancers in many malignant tumors [49-51]. Therefore, distinguishing the extent of TIL infiltration is critical for deconstructing the immunosuppressive microenvironment. Our study confirmed that the expression levels of the immune markers $CD3^+$, $CD8^+$, and $CD45RO^+$ were significantly associated with recurrence (Figure S16). Interestingly, there was a strong correlation between the locations of the TILs. Particularly, $TILs_{(IM)}$ showed a more significant correlation. Our data suggest that IRS is associated with the effect of $CD8^+_{(IM)}$ TILs. Increased $CD8^+_{(IM)}$ TIL infiltration enhances local antitumor activity in low- and moderate-risk populations. With an increase in IRS, $CD8^+_{(IM)}$ TIL infiltration tended to decrease. However, this trend was reversed in the high-risk group. Despite the increased infiltration of $CD8^+_{(IM)}$ TILs in the high-risk group, PD-1 and TIM-3 overexpression led to exhaustion of most $CD8^+_{(IM)}$ TILs, which represented the inhibition of the antitumor effect of CTLs [36-38]. Due to the suppression of the local immune response, patients with GC still have micrometastasis after adjuvant chemotherapy, which may explain why patients with GC with high IRS have higher risk of recurrence (especially the recurrence of perigastric lymph nodes).

Adjuvant chemotherapy is the standard treatment for patients with advanced GC after surgery. However, the efficacy of chemotherapy, together with its direct cytoinhibitory/cytotoxic effects, can also be affected by (re)activation of the antitumor immune response [52, 53]. In our study, IRS was able to predict the sensitivity of patients with GC to adjuvant chemotherapy. In the moderate-risk group, in which immune function was not completely suppressed, postoperative adjuvant chemotherapy significantly reduced the recurrence rate. However, chemotherapy was ineffective in the high-risk group of immunosuppressed patients. For these patients, new therapies must be developed to reduce postoperative recurrence rates. Most patients who respond to immunotherapy present with so-called “hot” tumors [54], which have a high level of immune cell infiltration; however, the expression of inhibitory receptors (e.g., PD-1 and TIM-3) in immune cells inhibits the antitumor effect [17, 19, 54]. Our study showed that patients with GC in the IRS high-risk group displayed this characteristic. Therefore, we speculate that the prognosis of patients with GC in the high-risk group may be improved by immunotherapy. However, our study had some limitations. First, this was a retrospective study, and the follow-up time of the patients receiving immunotherapy in our center was only 1 year; hence, we do not have corresponding data to verify the abovementioned hypothesis.

In conclusion, we constructed a model based on six immunosuppressive indicators to assess

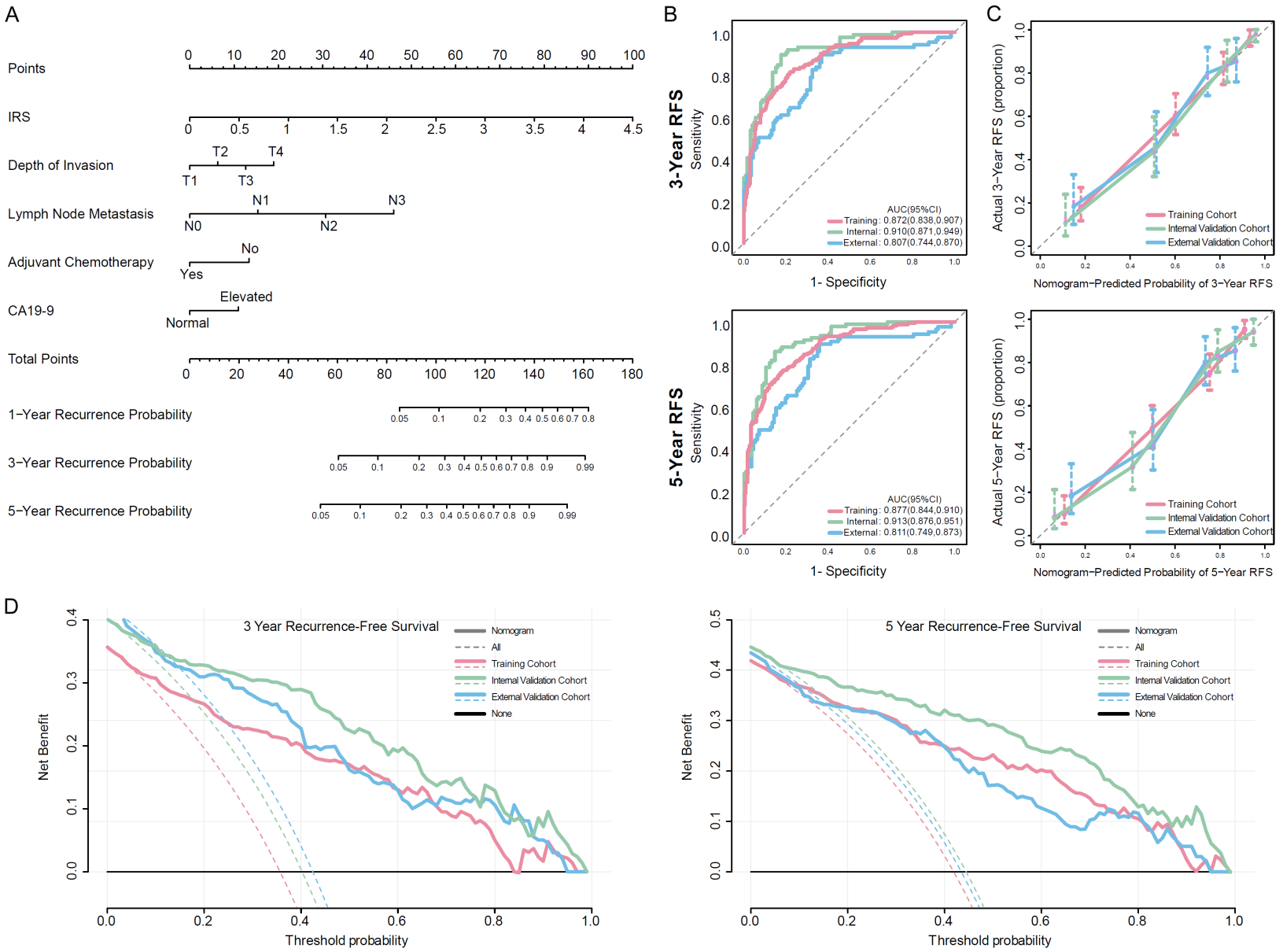

Figure 7. IRS-based nomogram to predict recurrence probability. A. Nomogram based on the IRS to predict postoperative recurrence. B-D. Time-dependent ROC curve, calibration curve, and DCA for the nomogram in the training cohort and internal and external validation cohorts.

the risk of recurrence in patients with GC. The predictive properties of this model can help surgeons customize treatment plans, including postoperative follow-up, examination, and treatment plans. For low-risk patients, the benefit of chemotherapy is not significant and the decision to administrate chemotherapy should be made according to the patient's condition. For patients in the moderate-risk group, adjuvant chemotherapy is recommended after surgery to reduce the risk of tumor recurrence. In the high-risk group, patients with GC who failed to respond to chemotherapy alone may benefit from immunotherapy. Simultaneously, patients in the high-risk group need to strengthen follow-up frequency to pay attention to the existence of recurrence, focusing on the possibility of locoregional recurrence (especially in the perigastric lymph node area) after surgery. This is because patients in our analysis in the regional group (red circle in **Figure 4A**) and lymph node group (red circle in Figure S10C) showed other recurrence patterns. According to our results, IRS can help make broad clinical decisions and provide more opportunities to treat resectable GC.

Acknowledgements

This work was supported by the Science and Technology Innovation Joint Fund Project of Fujian Province (No. 2019Y9098 and No. 2019Y9089). We thank the members of the Key Laboratory of the Ministry of Education for Gastrointestinal Cancer for their helpful comments and suggestions.

Disclosure of conflict of interest

None.

Abbreviations

AJCC, American Joint Committee on Cancer; AUC, Area under the curve; CI, Confidence interval; CT, Center of tumor; DCA, Decision curve analysis; DFS, Diseases-free survival; EBV, Epstein-Barr virus; GC, Gastric cancer; HR, Hazard ratio; IM, Invasive margin; IRS, Immunosuppressive recurrence score; LASSO, Least absolute shrinkage and selection operator; MDSCs, Myeloid-derived suppressor cells; MSI, Microsatellite instability; RFS, Recurrence-free survival; PD-1, Programmed cell death protein 1; PD-L1, Programmed cell death 1 ligand 1; ROC, Receiver operator characteristic; TAMs, Tumor-associated macrophages; TILs, Tumor-infiltrating lymphocytes; TIM-3, T cell immunoglobulin and mucin domain-containing protein 3.

Address correspondence to: Jianwei Xie and Changming Huang, Department of Gastric Surgery, Fujian Medical University Union Hospital, No. 29 Xinquan Road, Fuzhou 350001, Fujian, China. E-mail: xjwhw2019@163.com (JWX); hcmlr2002@163.com (CMH)

References

[1] Deng J, Liang H, Wang D, Sun D, Pan Y and Liu Y. Investigation of the recurrence patterns of gastric cancer following a curative resection. Surg Today 2011; 41: 210-215.

[2] D'Angelica M, Gonen M, Brennan MF, Turnbull AD, Bains M and Karpeh MS. Patterns of initial recurrence in completely resected gastric adenocarcinoma. Ann Surg 2004; 240: 808-816.

[3] Wu C, Lo S, Shen K, Hsieh M, Chen J, Chiang J, Lin H, Li A and Lui W. Incidence and factors associated with recurrence patterns after intended curative surgery for gastric cancer. World J Surg 2003; 27: 153-158.

[4] Schwarz R and Zagala-Nevarez K. Recurrence patterns after radical gastrectomy for gastric cancer: prognostic factors and implications for postoperative adjuvant therapy. Ann Surg Oncol 2002; 9: 394-400.

[5] Yoo C, Noh S, Shin D, Choi S and Min J. Recurrence following curative resection for gastric carcinoma. Br J Surg 2000; 87: 236-242.

[6] Sakuramoto S, Sasako M, Yamaguchi T, Kinoshita T, Fujii M, Nashimoto A, Furukawa H, Nakajima T, Ohashi Y, Imamura H, Higashino M, Yamamura Y, Kurita A and Arai K. Adjuvant chemotherapy for gastric cancer with S-1, an oral fluoropyrimidine. N Engl J Med 2007; 357: 1810-1820.

[7] Smyth E, Verheij M, Allum W, Cunningham D, Cervantes A and Arnold D. Gastric cancer: ESMO Clinical Practice Guidelines for diagnosis, treatment and follow-up. Ann Oncol 2016; 27: v38-v49.

[8] Zitvogel L, Kepp O and Kroemer G. Immune parameters affecting the efficacy of chemotherapeutic regimens. Nature reviews. Nat Rev Clin Oncol 2011; 8: 151-160.

[9] Casares N, Pequignot M, Tesniere A, Ghiringhelli F, Roux S, Chaput N, Schmitt E, Hamai A, Hervas-Stubbs S, Obeid M, Coutant F, Métivier D, Pichard E, Aucouturier P, Pierron G, Garrido C, Zitvogel L and Kroemer G. Caspase-dependent immunogenicity of doxorubicin-induced tumor cell death. J Exp Med 2005; 202: 1691-1701.

[10] Weber JS, D'Angelo SP, Minor D, Hodi FS, Gutzmer R, Neyns B, Hoeller C, Khushalani NI, Miller WH Jr, Lao CD, Linette GP, Thomas L, Lorigan P, Grossmann KF, Hassel JC, Maio M, Sznol M, Ascierto PA, Mohr P, Chmielowski B, Bryce A, Svane IM, Grob JJ, Krackhardt AM, Horak C, Lambert A, Yang AS and Larkin J. Nivolumab versus chemotherapy in patients with advanced melanoma who progressed after anti-CTLA-4 treatment (CheckMate 037): a randomised, controlled, open-label, phase 3 trial. Lancet Oncol 2015; 16: 375-384.

[11] Kanda S, Goto K, Shiraishi H, Kubo E, Tanaka A, Utsumi H, Sunami K, Kitazono S, Mizugaki H, Horinouchi H, Fujiwara Y, Nokihara H, Yamamoto N, Hozumi H and Tamura T. Safety and efficacy of nivolumab and standard chemotherapy drug combination in patients with advanced non-small-cell lung cancer: a four arms phase Ib study. Ann Oncol 2016; 27: 2242-2250.

[12] Nanda R, Liu MC, Yau C, Shatsky R, Pusztai L, Wallace A, Chien AJ, Forero-Torres A, Ellis E, Han H, Clark A, Albain K, Boughey JC, Jaskowiak NT, Elias A, Isaacs C, Kemmer K, Helsten T, Majure M, Stringer-Reasor E, Parker C, Lee MC, Haddad T, Cohen RN, Asare S, Wilson A, Hirst GL, Singhrao R, Steeg K, Asare A, Matthews JB, Berry S, Sanil A, Schwab R, Symmans WF, van't Veer L, Yee D, DeMichele A, Hylton NM, Melisko M, Perlmutter J, Rugo HS, Berry DA and Esserman LJ. Effect of pembrolizumab plus neoadjuvant chemotherapy on pathologic complete response in women with early-stage breast cancer: an analysis of the ongoing phase 2 adaptively randomized I-SPY2 trial. JAMA Oncol 2020; 6: 676-684.

[13] Burtness B, Harrington KJ, Greil R, Soulières D, Tahara M, de Castro G Jr, Psyrri A, Basté N, Neupane P, Bratland Å, Fuereder T, Hughes BGM, Mesía R, Ngamphaiboon N, Rordorf T, Wan Ishak WZ, Hong RL, González Mendoza R, Roy A, Zhang Y, Gumuscu B, Cheng JD, Jin F and Rischin D; KEYNOTE-048 Investigators. Pembrolizumab alone or with chemotherapy versus cetuximab with chemotherapy for recurrent or metastatic squamous cell carcinoma of the head and neck (KEYNOTE-048): a randomised, open-label, phase 3 study. Lancet 2019; 394: 1915-1928.

[14] Gutzmer R, Stroyakovskiy D, Gogas H, Robert C, Lewis K, Protsenko S, Pereira RP, Eigentler T, Rutkowski P, Demidov L, Manikhas GM, Yan Y, Huang KC, Uyei A, McNally V, McArthur GA and Ascierto PA. Atezolizumab, vemurafenib, and cobimetinib as first-line treatment for unresectable advanced $BRAF^{V600}$ mutation-positive melanoma (IMspire150): primary analysis of the randomised, double-blind, placebo-controlled, phase 3 trial. Lancet 2020; 395: 1835-1844.

[15] Robert C, Ribas A, Schachter J, Arance A, Grob JJ, Mortier L, Daud A, Carlino MS, McNeil CM, Lotem M, Larkin JMG, Lorigan P, Neyns B, Blank CU, Petrella TM, Hamid O, Su SC, Krepler C, Ibrahim N and Long GV. Pembrolizumab versus ipilimumab in advanced melanoma (KEYNOTE-006): post-hoc 5-year results from an open-label, multicentre, randomised, controlled, phase 3 study. Lancet Oncol 2019; 20: 1239-1251.

[16] Schildberg F, Klein S, Freeman G and Sharpe A. Coinhibitory pathways in the B7-CD28 ligand-receptor family. Immunity 2016; 44: 955-972.

[17] Chen YP, Zhang Y, Lv JW, Li YQ, Wang YQ, He QM, Yang XJ, Sun Y, Mao YP, Yun JP, Liu N and Ma J. Genomic analysis of tumor microenvironment immune types across 14 solid cancer types: immunotherapeutic implications. Theranostics 2017; 7: 3585-3594.

[18] Zeng D, Li M, Zhou R, Zhang J, Sun H, Shi M, Bin J, Liao Y, Rao J and Liao W. Tumor microenvironment characterization in gastric cancer identifies prognostic and immunotherapeutically relevant gene signatures. Cancer Immunol Res 2019; 7: 737-750.

[19] Tumeh PC, Harview CL, Yearley JH, Shintaku IP, Taylor EJ, Robert L, Chmielowski B, Spasic M, Henry G, Ciobanu V, West AN, Carmona M, Kivork C, Seja E, Cherry G, Gutierrez AJ, Grogan TR, Mateus C, Tomasic G, Glaspy JA, Emerson RO, Robins H, Pierce RH, Elashoff DA, Robert C and Ribas A. PD-1 blockade induces responses by inhibiting adaptive immune resistance. Nature 2014; 515: 568-571.

[20] Wang M, Huang YK, Kong JC, Sun Y, Tantalo DG, Yeang HXA, Ying L, Yan F, Xu D, Halse H, Di Costanzo N, Gordon IR, Mitchell C, Mackay LK, Busuttil RA, Neeson PJ and Boussioutas A. High-dimensional analyses reveal a distinct role of T-cell subsets in the immune microenvironment of gastric cancer. Clin Transl Immunology 2020; 9: e1127.

[21] Sun Y, Wu L, Zhong Y, Zhou K, Hou Y, Wang Z, Zhang Z, Xie J, Wang C, Chen D, Huang Y, Wei X, Shi Y, Zhao Z, Li Y, Guo Z, Yu Q, Xu L, Volpe G, Qiu S, Zhou J, Ward C, Sun H, Yin Y, Xu X, Wang X, Esteban MA, Yang H, Wang J, Dean M, Zhang Y, Liu S, Yang X and Fan J. Single-cell landscape of the ecosystem in early-relapse hepatocellular carcinoma. Cell 2021; 184: 404-421, e16.

[22] Jeong YM, Cho H, Kim TM, Kim Y, Jeon S, Bychkov A and Jung CK. CD73 overexpression promotes progression and recurrence of papillary thyroid carcinoma. Cancers (Basel) 2020; 12: 3042.

[23] Hutchinson K, Yost S, Chang C, Johnson R, Carr A, McAdam P, Halligan D, Chang C, Schmolze D, Liang J and Yuan Y. Comprehensive profiling of poor-risk paired primary and recurrent triple-negative breast cancers reveals immune phenotype shifts. Clin Cancer Res 2020; 26: 657-668.

[24] Corredor G, Wang X, Zhou Y, Lu C, Fu P, Syrigos K, Rimm DL, Yang M, Romero E, Schalper KA, Velcheti V and Madabhushi A. Spatial architecture and arrangement of tumor-infiltrating lymphocytes for predicting likelihood of recurrence in early-stage non-small cell lung cancer. Clin Cancer Res 2019; 25: 1526-1534.

[25] Pharmaceutical O. ONO submits supplemental application for approval for opdivo® (nivolumab) to expand the use for treatment of previously untreated unresectable advanced or recurrent gastric cancer in Japan. 2020; https://www.ono.co.jp/eng/news/pdf/sm_cn200514.pdf, Accessed Aug 14, 2020.

[26] Squibb BM. Press release: CheckMate 649, a phase 3 trial evaluating opdivo (nivolumab) plus chemotherapy vs chemotherapy, meets primary endpoints demonstrating superior overall survival and progressionfree survival in firstline treatment of gastric and esophageal cancers. 2020; https://news.bms.com/ press-release/corporatefinancialnews/checkmate-649-phase-3-trial-evaluatingopdivonivolumab-plusc, Accessed Aug 14, 2020.

[27] Wang JB, Li P, Liu XL, Zheng QL, Ma YB, Zhao YJ, Xie JW, Lin JX, Lu J, Chen QY, Cao LL, Lin M, Liu LC, Lian NZ, Yang YH, Huang CM and Zheng CH. An immune checkpoint score system for prognostic evaluation and adjuvant chemotherapy selection in gastric cancer. Nat Commun 2020; 11: 6352.

[28] Freeman G, Long A, Iwai Y, Bourque K, Chernova T, Nishimura H, Fitz L, Malenkovich N, Okazaki T, Byrne M, Horton H, Fouser L, Carter L, Ling V, Bowman M, Carreno B, Collins M, Wood C and Honjo T. Engagement of the PD-1 immunoinhibitory receptor by a novel B7 family member leads to negative regulation of lymphocyte activation. J Exp Med 2000; 192: 1027-1034.

[29] Okoye I, Xu L, Motamedi M, Parashar P, Walker J and Elahi S. Galectin-9 expression defines exhausted T cells and impaired cytotoxic NK cells in patients with virus-associated solid tumors. J Immunother Cancer 2020; 8: e001849.

[30] Yang F, Zeng Z, Li J, Ren X and Wei F. TIM-3 and CEACAM1 are prognostic factors in head and neck squamous cell carcinoma. Front Mol Biosci 2021; 8: 619765.

[31] Gorvel L and Olive D. Targeting the "PVR-TIGIT axis" with immune checkpoint therapies. F1000Res 2020; 9: F1000 Faculty Rev-354.

[32] Zheng B, Wang D, Qiu X, Luo G, Wu T, Yang S, Li Z, Zhu Y, Wang S, Wu R, Sui C, Gu Z, Shen S, Jeong S, Wu X, Gu J, Wang H and Chen L. Trajectory and functional analysis of PD-1(high) CD4(+)CD8(+) T cells in hepatocellular carcinoma by single-cell cytometry and transcriptome sequencing. Adv Sci (Weinh) 2020; 7: 2000224.

[33] Kim K, Lee K, Cho H, Kim Y, Yang H, Kim W and Kang G. Prognostic implications of tumor-infiltrating FoxP3+ regulatory T cells and CD8+ cytotoxic T cells in microsatellite-unstable gastric cancers. Hum Pathol 2014; 45: 285-293.

[34] Chiaravalli A, Feltri M, Bertolini V, Bagnoli E, Furlan D, Cerutti R, Novario R and Capella C. Intratumour T cells, their activation status and survival in gastric carcinomas characterised for microsatellite instability and Epstein-Barr virus infection. Virchows Arch 2006; 448: 344-353.

[35] Liu K, Yang K, Wu B, Chen H, Chen X, Chen X, Jiang L, Ye F, He D, Lu Z, Xue L, Zhang W, Li Q, Zhou Z, Mo X and Hu J. Tumor-infiltrating immune cells are associated with prognosis of gastric cancer. Medicine (Baltimore) 2015; 94: e1631.

[36] Henao-Tamayo M, Irwin S, Shang S, Ordway D and Orme I. T lymphocyte surface expression of exhaustion markers as biomarkers of the efficacy of chemotherapy for tuberculosis. Tuberculosis (Edinb) 2011; 91: 308-313.

[37] Liu J, Zhang S, Hu Y, Yang Z, Li J, Liu X, Deng L, Wang Y, Zhang X, Jiang T and Lu X. Targeting PD-1 and Tim-3 pathways to reverse CD8 T-cell exhaustion and enhance ex vivo t-cell responses to autologous dendritic/tumor vaccines. J Immunother 2016; 39: 171-180.

[38] Xu B, Yuan L, Gao Q, Yuan P, Zhao P, Yuan H, Fan H, Li T, Qin P, Han L, Fang W and Suo Z. Circulating and tumor-infiltrating Tim-3 in patients with colorectal cancer. Oncotarget 2015; 6: 20592-20603.

[39] Li X, Yao W, Yuan Y, Chen P, Li B, Li J, Chu R, Song H, Xie D, Jiang X and Wang H. Targeting of tumour-infiltrating macrophages via CCL2/CCR2 signalling as a therapeutic strategy against hepatocellular carcinoma. Gut 2017; 66: 157-167.

[40] Zhou C, Weng J, Liu C, Zhou Q, Chen W, Hsu J, Sun J, Atyah M, Xu Y, Shi Y, Shen Y, Dong Q, Hung M and Ren N. High RPS3A expression correlates with low tumor immune cell infiltration and unfavorable prognosis in hepatocellular carcinoma patients. Am J Cancer Res 2020; 10: 2768-2784.

[41] Huber V, Camisaschi C, Berzi A, Ferro S, Lugini L, Triulzi T, Tuccitto A, Tagliabue E, Castelli C and Rivoltini L. Cancer acidity: an ultimate frontier of tumor immune escape and a novel

target of immunomodulation. Semin Cancer Biol 2017; 43: 74-89.
[42] He W, Zhang H, Han F, Chen X, Lin R, Wang W, Qiu H, Zhuang Z, Liao Q, Zhang W, Cai Q, Cui Y, Jiang W, Wang H and Ke Z. CD155T/TIGIT signaling regulates CD8(+) T-cell metabolism and promotes tumor progression in human gastric cancer. Cancer Res 2017; 77: 6375-6388.
[43] Kim W, Chu TH, Nienhuser H, Jiang Z, Del Portillo A, Remotti HE, White RA, Hayakawa Y, Tomita H, Fox JG, Drake CG and Wang TC. PD-1 signaling promotes tumor-infiltrating myeloid-derived suppressor cells and gastric tumorigenesis in mice. Gastroenterology 2020; 160: 781-796.
[44] Thompson E, Zahurak M, Murphy A, Cornish T, Cuka N, Abdelfatah E, Yang S, Duncan M, Ahuja N, Taube J, Anders R and Kelly R. Patterns of PD-L1 expression and CD8 T cell infiltration in gastric adenocarcinomas and associated immune stroma. Gut 2017; 66: 794-801.
[45] Liu Y, Liang X, Dong W, Fang Y, Lv J, Zhang T, Fiskesund R, Xie J, Liu J, Yin X, Jin X, Chen D, Tang K, Ma J, Zhang H, Yu J, Yan J, Liang H, Mo S, Cheng F, Zhou Y, Zhang H, Wang J, Li J, Chen Y, Cui B, Hu Z, Cao X, Xiao-Feng Qin F and Huang B. Tumor-repopulating cells induce PD-1 expression in CD8 T cells by transferring kynurenine and AhR activation. Cancer cell 2018; 33: 480-494.
[46] Cai T, Nesi G, Boddi V, Mazzoli S, Dal Canto M and Bartoletti R. Prognostic role of the tumor-associated tissue inflammatory reaction in transitional bladder cell carcinoma. Oncol Rep 2006; 16: 329-334.
[47] Bremnes R, Al-Shibli K, Donnem T, Sirera R, Al-Saad S, Andersen S, Stenvold H, Camps C and Busund L. The role of tumor-infiltrating immune cells and chronic inflammation at the tumor site on cancer development, progression, and prognosis: emphasis on non-small cell lung cancer. J Thorac Oncol 2011; 6: 824-833.
[48] Job S, Rapoud D, Dos Santos A, Gonzalez P, Desterke C, Pascal G, Elarouci N, Ayadi M, Adam R, Azoulay D, Castaing D, Vibert E, Cherqui D, Samuel D, Sa Cuhna A, Marchio A, Pineau P, Guettier C, de Reyniès A and Faivre J. Identification of four immune subtypes characterized by distinct composition and functions of tumor microenvironment in intrahepatic cholangiocarcinoma. Hepatology 2020; 72: 965-981.
[49] Quan H, Shan Z, Liu Z, Liu S, Yang L, Fang X, Li K, Wang B, Deng Z, Hu Y, Yao Z, Huang J, Yu J, Xia K, Tang Z and Fang L. The repertoire of tumor-infiltrating lymphocytes within the microenvironment of oral squamous cell carcinoma reveals immune dysfunction. Cancer Immunol Immunother 2020; 69: 465-476.
[50] Chen F, Yang Y, Zhao Y, Pei L and Yan H. Immune infiltration profiling in nonsmall cell lung cancer and their clinical significance: study based on gene expression measurements. DNA Cell Biol 2019; 38: 1387-1401.
[51] Takami H, Fukushima S, Aoki K, Satomi K, Narumi K, Hama N, Matsushita Y, Fukuoka K, Yamasaki K, Nakamura T, Mukasa A, Saito N, Suzuki T, Yanagisawa T, Nakamura H, Sugiyama K, Tamura K, Maehara T, Nakada M, Nonaka M, Asai A, Yokogami K, Takeshima H, Iuchi T, Kanemura Y, Kobayashi K, Nagane M, Kurozumi K, Yoshimoto K, Matsuda M, Matsumura A, Hirose Y, Tokuyama T, Kumabe T, Ueki K, Narita Y, Shibui S, Totoki Y, Shibata T, Nakazato Y, Nishikawa R, Matsutani M and Ichimura K; Intracranial Germ Cell Tumor Genome Analysis Consortium (the iGCT Consortium). Intratumoural immune cell landscape in germinoma reveals multipotent lineages and exhibits prognostic significance. Neuropathol Appl Neurobiol 2020; 46: 111-124.
[52] Galluzzi L, Buqué A, Kepp O, Zitvogel L and Kroemer G. Immunological effects of conventional chemotherapy and targeted anticancer agents. Cancer Cell 2015; 28: 690-714.
[53] Coffelt S and de Visser K. Immune-mediated mechanisms influencing the efficacy of anticancer therapies. Trends Immunol 2015; 36: 198-216.
[54] Galon J and Bruni D. Approaches to treat immune hot, altered and cold tumours with combination immunotherapies. Nature reviews. Nat Rev Drug Discov 2019; 18: 197-218.

Supplementary methods

Patient information

Gastric tissue specimens, including tumor tissues of the stomach and adjacent non-tumor tissues, which were fixed in formalin and embedded in paraffin. The inclusion criteria were as follows: (a) histological identification of gastric cancer (GC), (b) no other malignant tumors or distant metastases, (c) availability of follow-up data and clinicopathological characteristics, and (d) TNM staging of GC tumors according to the 2010 International Union Against Cancer guidelines. The exclusion criteria were as follows: (1) death within 1 month of surgery and (2) chemotherapy or radiotherapy before surgery. All participants with advanced GC routinely received fluorine-based chemotherapy. Informed consent was obtained from all participants.

Follow-up

All participants were followed up every 3 months during the first year and every 6 months thereafter. All surviving patients were followed up for >5 years. Overall survival was defined as the time from surgery to the last follow-up (October 2020), time of death, or database deadline (the time lost during follow-up). For patients with recurrence, recurrence-free survival was defined as the time from surgery to the first recurrence, while for patients without recurrence, recurrence-free survival was defined as the time from surgery to the last follow-up. Follow-up was conducted by clinicians from the three centers according to the uniform standards of the Japanese Statute. The overall loss to follow-up rate was 4.4%.

Definition of microsatellite instability (MSI) status

The scoring criteria (**Figure S3**) were at least one missing mismatch repair generelated protein, interpreted as deficient mismatch repair (dMMR), manifested as microsatellite instability (MSI)-H; no missing mismatch repair gene-related protein was interpreted as proficient MMR, manifested as MSI-L/MSS.

Multiplexed immunofluorescence staining and analysis

The formalin-fixed paraffin-embedded tissue sections were cut into 4 mm-thick sections, thawed at 70°C for 45 min, deparaffinized, and fixed with formaldehyde:methanol (1:10). Subsequently, in ethylenediaminetetraacetic acid buffer (pH 8.0), heat-induced antigen recovery was performed at 100% power in an 800 W standard microwave until the boiling point and then at 30% power for 15 min. The tissue sections were then cooled and washed in 0.02% Tris-buffered saline-Tween 20 (TBST) with gentle stirring. The sections were then blocked with blocking buffer (X0909; Dako) for 10 min at room temperature and then incubated with the primary antibody at 4°C overnight. Then, the horseradish peroxidase (HRP)-conjugated secondary antibody (Perkin-Elmer, USA) was incubated at room temperature for 1 h, and the tyramide-based HRP was activated at 37°C for 20 min. The stained signal was further amplified using Opal 540 Acetamide Signal Amplification (TSA) reagent (Perkin-Elmer, USA) and incubated with TSA at room temperature to allow covalent binding between the Pax-5 protein and different fluorophores, mediated by HRP-conjugated secondary antibodies. After this covalent reaction, additional antigen recovery (citrate buffer, pH 6.0) was performed for 20 min to remove the bound antibody. All steps were repeated in sequence for each primary antibody. After counterstaining with 4,6-diamidino-2-phenylindole (Life Technologies, UK) at room temperature, all sections were washed five times in 0.02% TBST for 5 min, each for 2 min, and stored in a 4°C lightproof box C until imaging. All nuclei were stained with DAPI.

Nomogram construction based on the immunosuppressive recurrence score

To build the nomogram, we selected meaningful clinicopathological characteristics (T stage, N stage, adjuvant chemotherapy, and CA19-9 level) using multivariate analysis and the immunosuppressive recurrence score to fit the Cox regression model with a stepwise backward method. The “rms” package of R was used to construct the fitting model and integrate the nomogram. The accuracy, reliability, and clinical usefulness of the nomogram was evaluated using time-dependent receiver operating characteristic (ROC), calibration, and decision curve analysis curves (DCA), respectively.

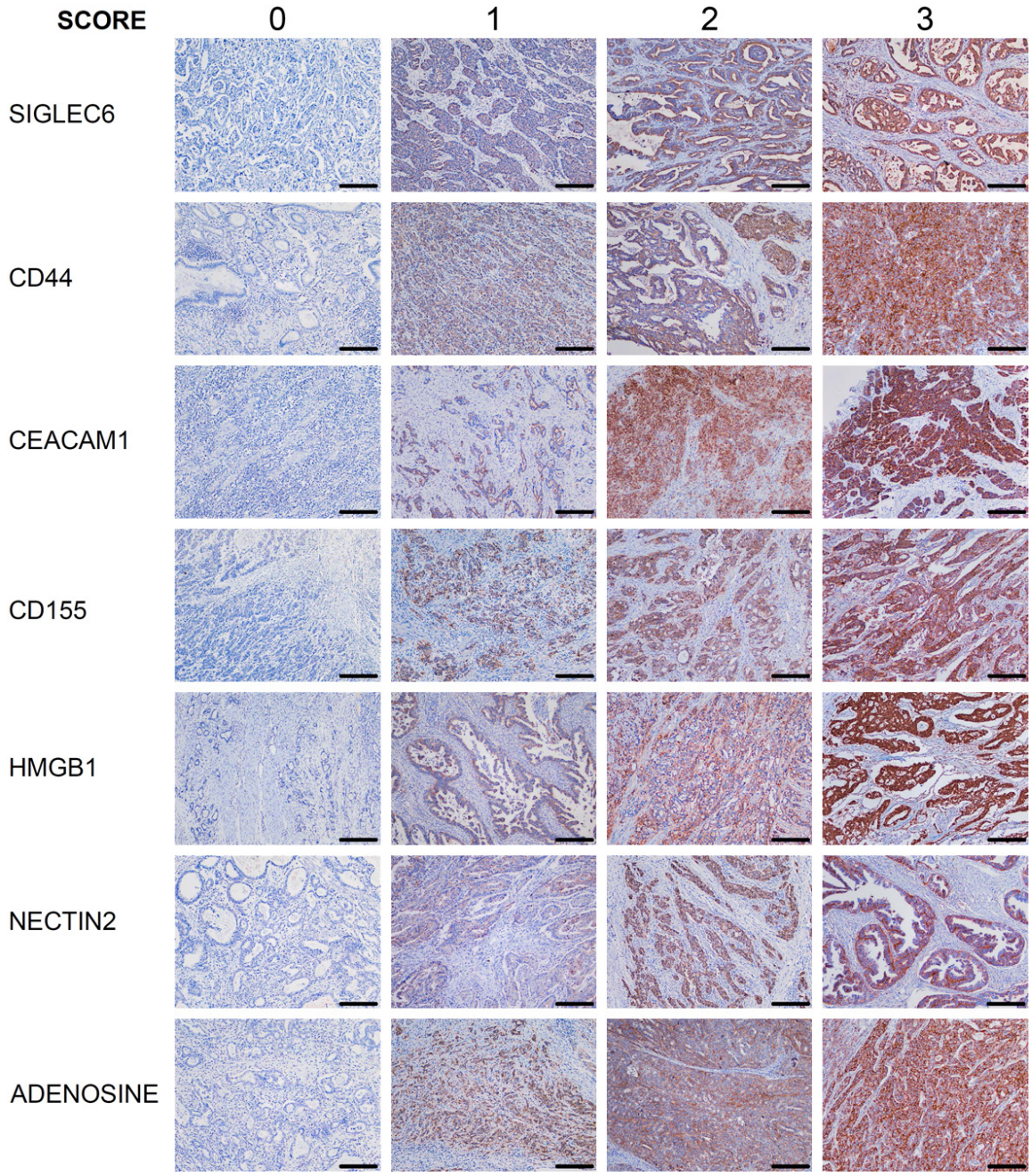

Figure S1. Immunohistochemical scoring criteria for seven immunosuppressive indicators. Scale bar =200 μm.

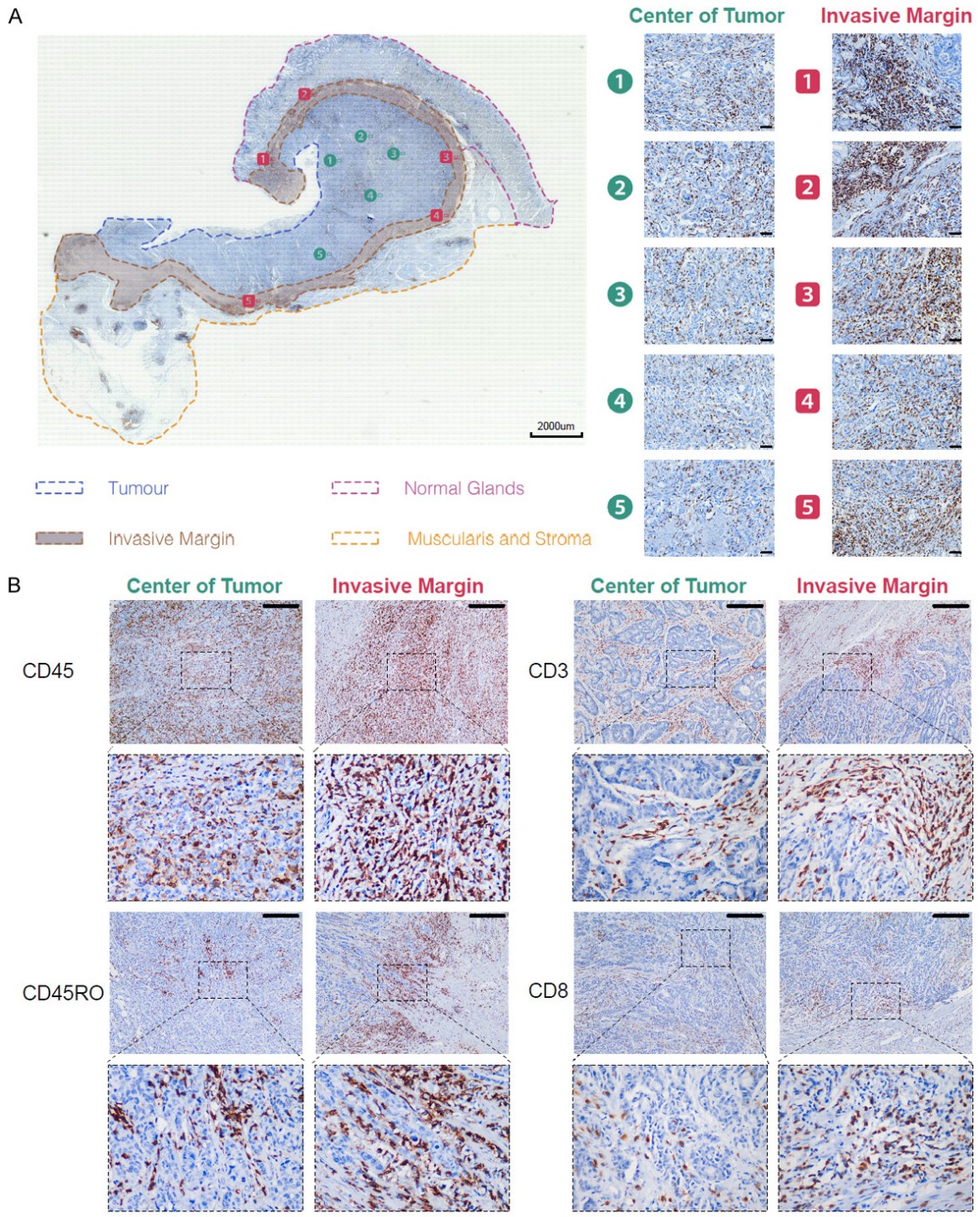

Figure S2. Immunohistochemical assessment of four immune biomarkers in patients with gastric cancer (GC). A. Schematic diagram of the selected field for immune cell count in the center of the tumor (CT) and invasive margin (IM). B. IHC staining for four immune biomarkers ($CD45^+$, $CD3^+$, $CD8^+$, $CD45RO^+$) in the CT and IM. Scale bar =200 μm.

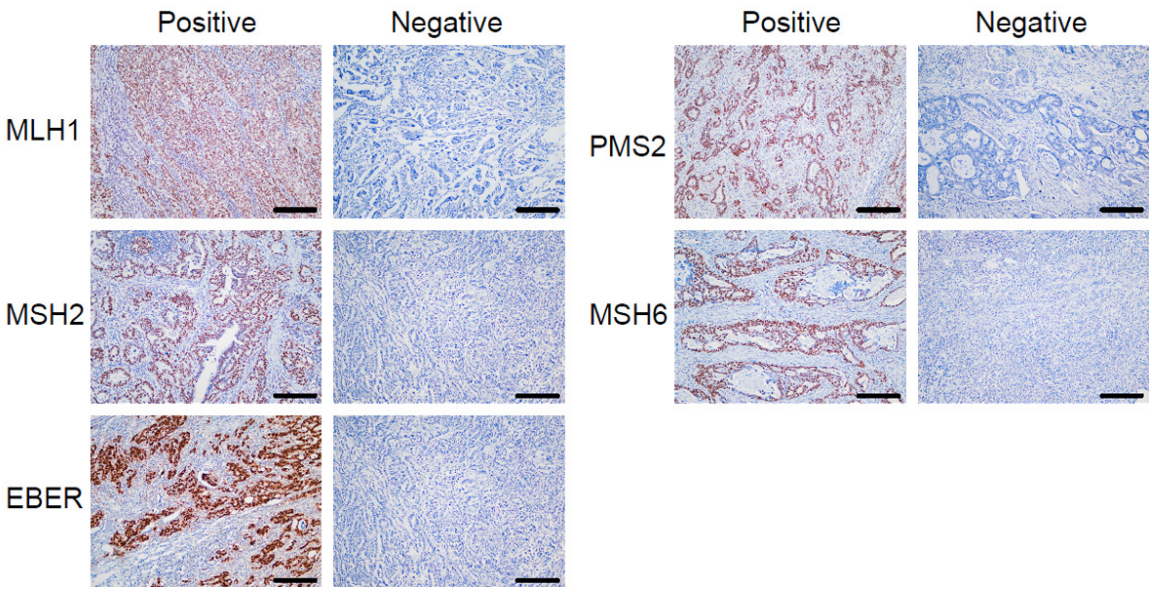

Figure S3. Immunohistochemical scoring criteria for microsatellite instability (MSI) status and in situ hybridization scoring criteria for Epstein-Barr virus (EBV) status. Scale bar =200 μm.

Table S1. Antibody Sources for Immunohistochemical and Multiplexed Immunofluorescence Staining

Markers	Antibody Source	Dilution	Species	Cellular localization	Application
SIGLEC6	ab38581, Abcam, UK	1:200	Rabbit monoclonal	Membranous	IHC
CD44	3570S, CST, USA	1:50	Mouse monoclonal	Membranous	IHC
CEACAM1	44464S, CST, USA	1:400	Rabbit monoclonal	Membranous	IHC
CD155	81254S, CST, USA	1:200	Rabbit monoclonal	Membranous	IHC
HMGB1	ab79823, Abcam, UK	1:400	Rabbit monoclonal	Membranous, nucleus and cytoplasm	IHC
NECTIN2	95333S, CST, USA	1:200	Rabbit monoclonal	Membranous	IHC
ADNEOSINE	ab40002, Abcam, UK	1:250	Goat monoclonal	Membranous	IHC
CD45	ab10558, Abcam, UK	1:200	Rabbit monoclonal	Membranous	IHC
CD3	ab16669, Abcam, UK	1:150	Rabbit monoclonal	Membranous	IHC
CD8	ab4055, Abcam, UK	1:200	Rabbit monoclonal	Membranous	IHC, IF
CD45RO	ab23, Abcam, UK	1:800	Mouse monoclonal	Membranous	IHC
PD-1	43248S, CST, USA	1:200	Mouse monoclonal	Membranous	IF
TIM-3	ab241332, Abcam, UK	1:100	Rabbit monoclonal	Membranous	IF
MLH1	ab92312, Abcam, UK	1:250	Rabbit monoclonal	Nucleus	IHC
MSH2	ab52266, Abcam, UK	1:250	Mouse monoclonal	Nucleus	IHC
MSH6	ab92471, Abcam, UK	1:250	Rabbit monoclonal	Nucleus	IHC
PMS2	ab110638, Abcam, UK	1:250	Rabbit monoclonal	Nucleus	IHC
EBER‡	ISH-6021, ZSGB-BIO, CHINA	-	-	Cytoplasm	-

‡Detection by in situ hybridization.

Immunosuppressive score to predict recurrence

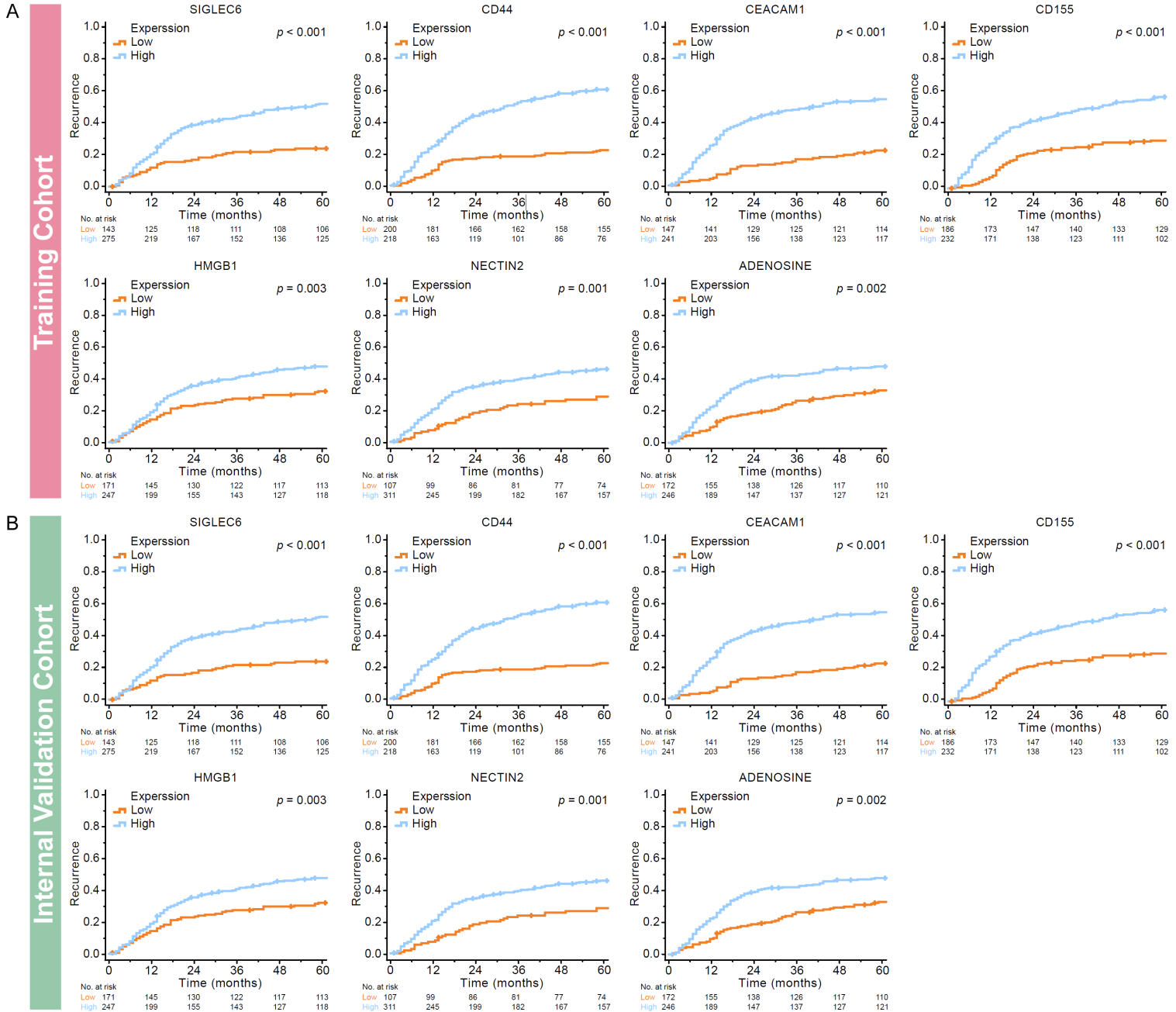

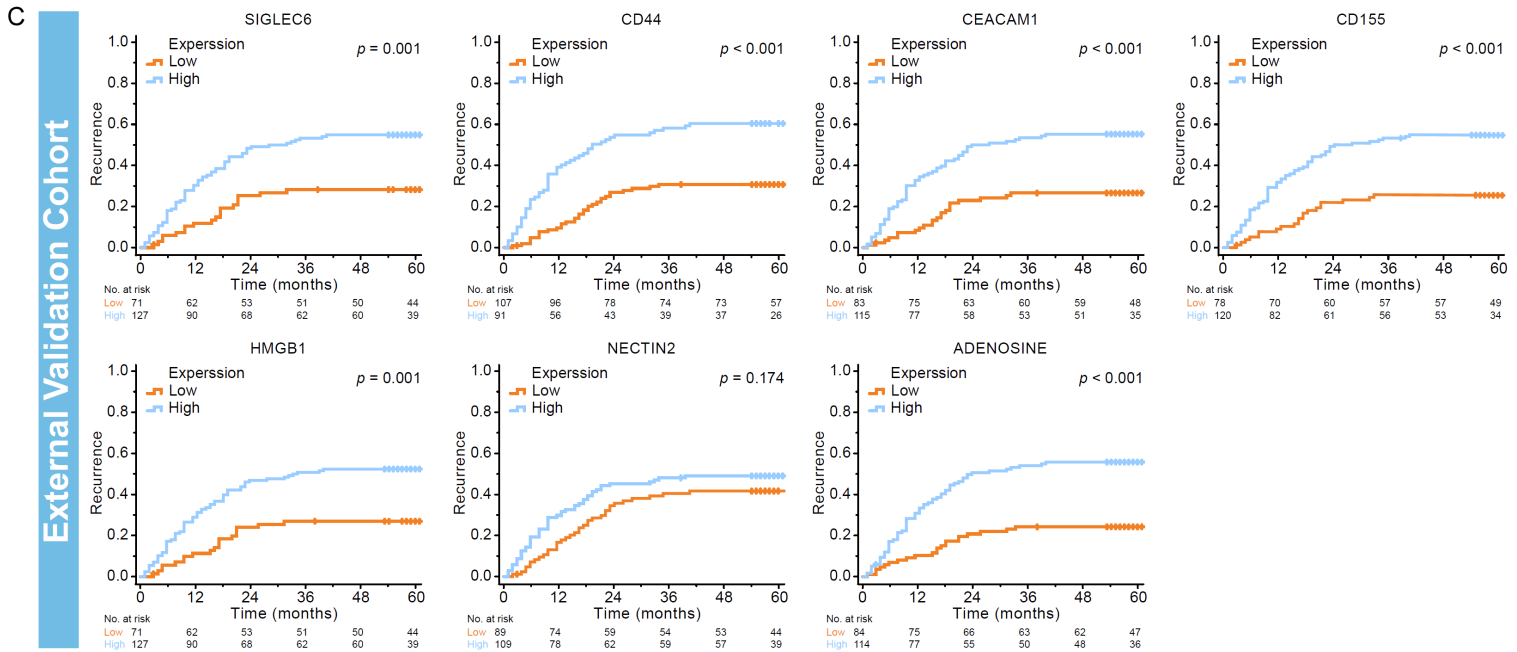

Figure S4. Seven immunosuppressive indicators are valuable in predicting gastric cancer recurrence after surgery. A. Training cohort. B. Internal validation cohort. C. External validation cohort. *P*-values were calculated using the log-rank test.

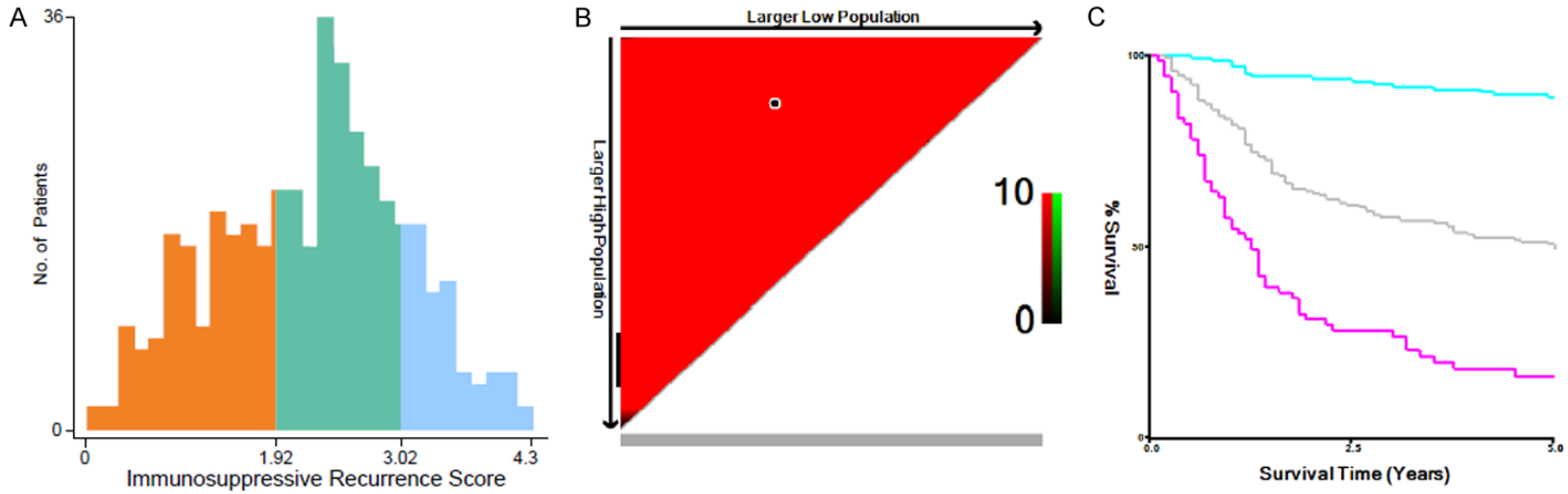

Figure S5. Cutoff values for the immunosuppressive recurrence score (IRS) derived using X-tile software.

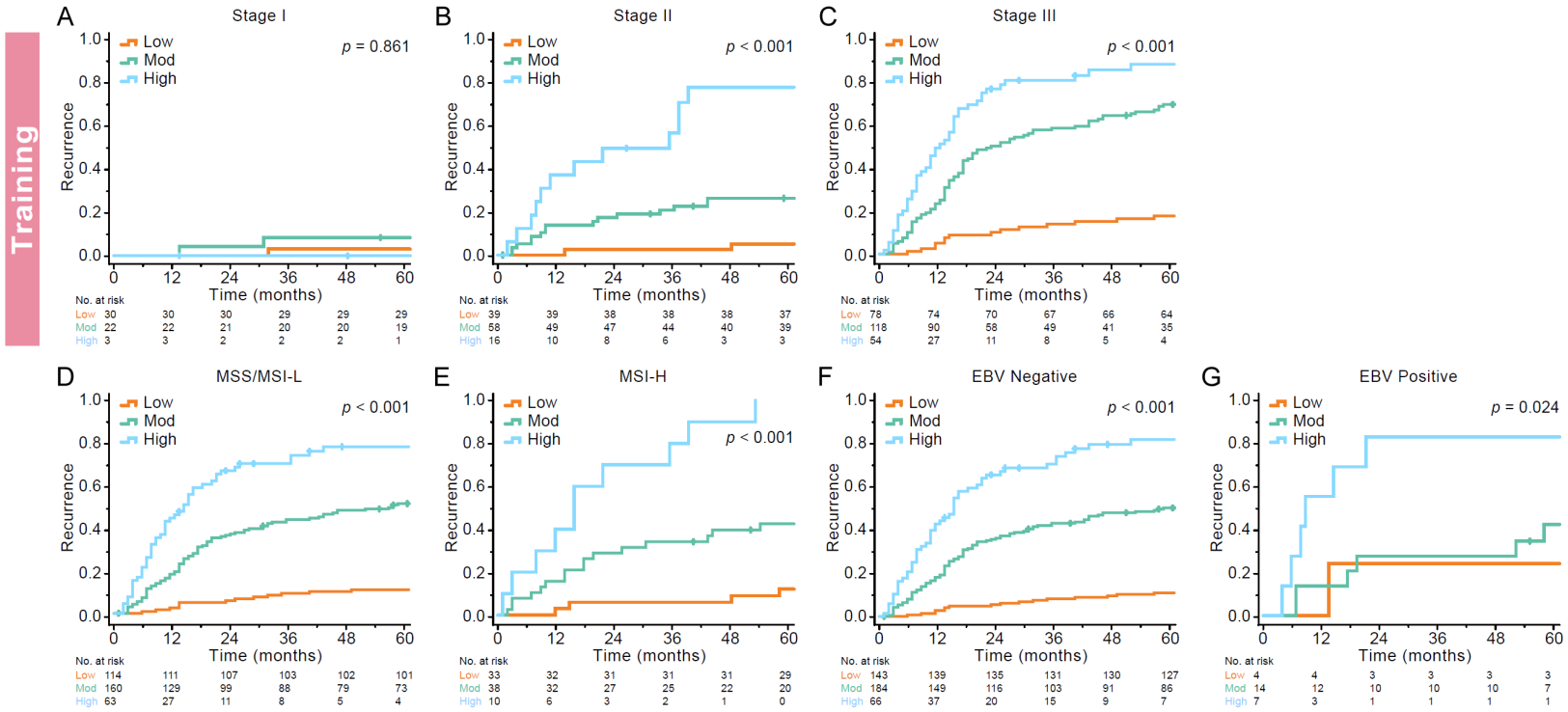

Figure S6. In the training cohort, stratified analysis showed that IRS was applicable to predict recurrence of postoperative GC patients with different clinicopathological characteristics. A-C. TNM stage. D, E. Microsatellite instability (MSI) status. F, G. Epstein-Barr virus (EBV) status. *P*-values were calculated using the log-rank test.

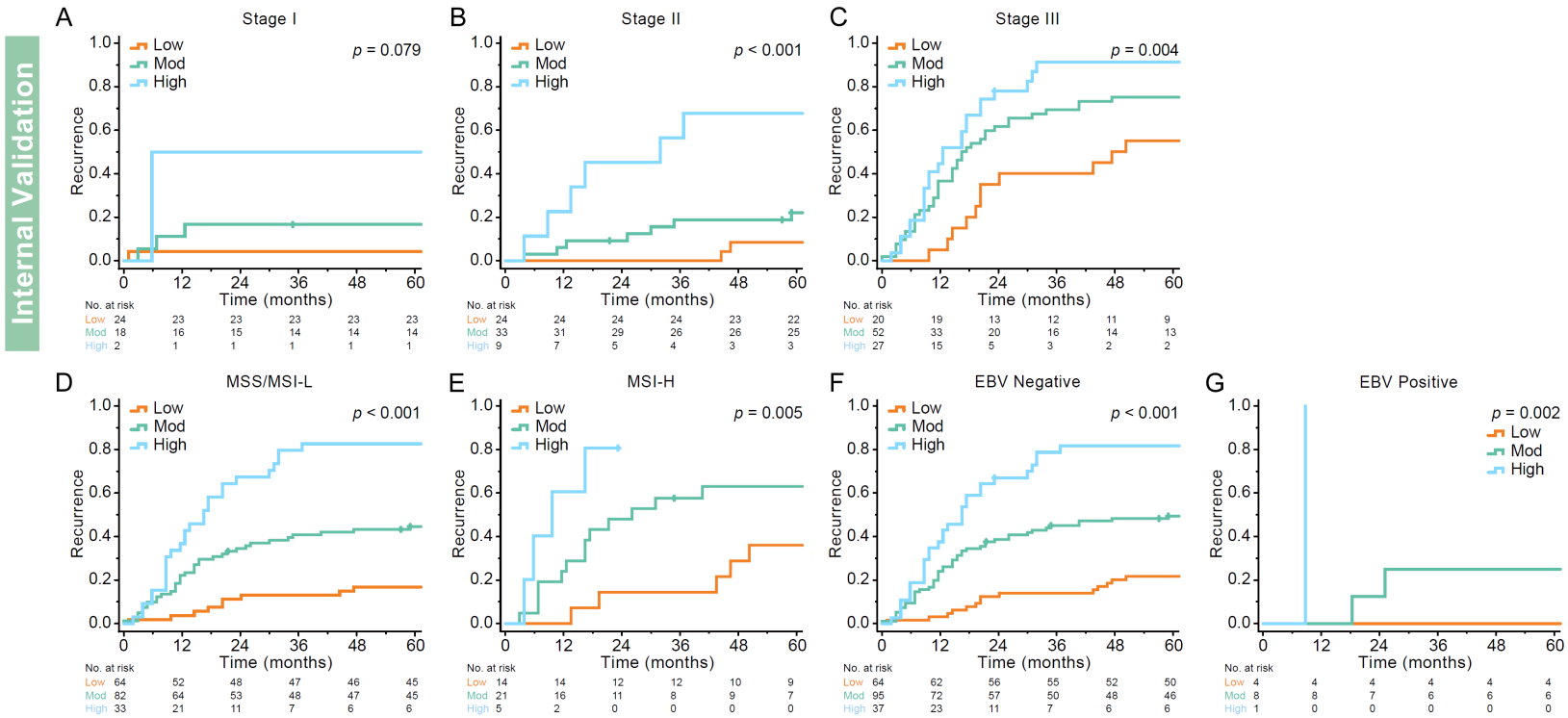

Figure S7. In the internal validation cohort, stratified analysis showed that IRS was applicable to predict recurrence of postoperative GC patients with different clinicopathological characteristics. A-C. TNM stage. D, E. Microsatellite instability (MSI) status. F, G. Epstein-Barr virus (EBV) status. *P*-values were calculated using the log-rank test.

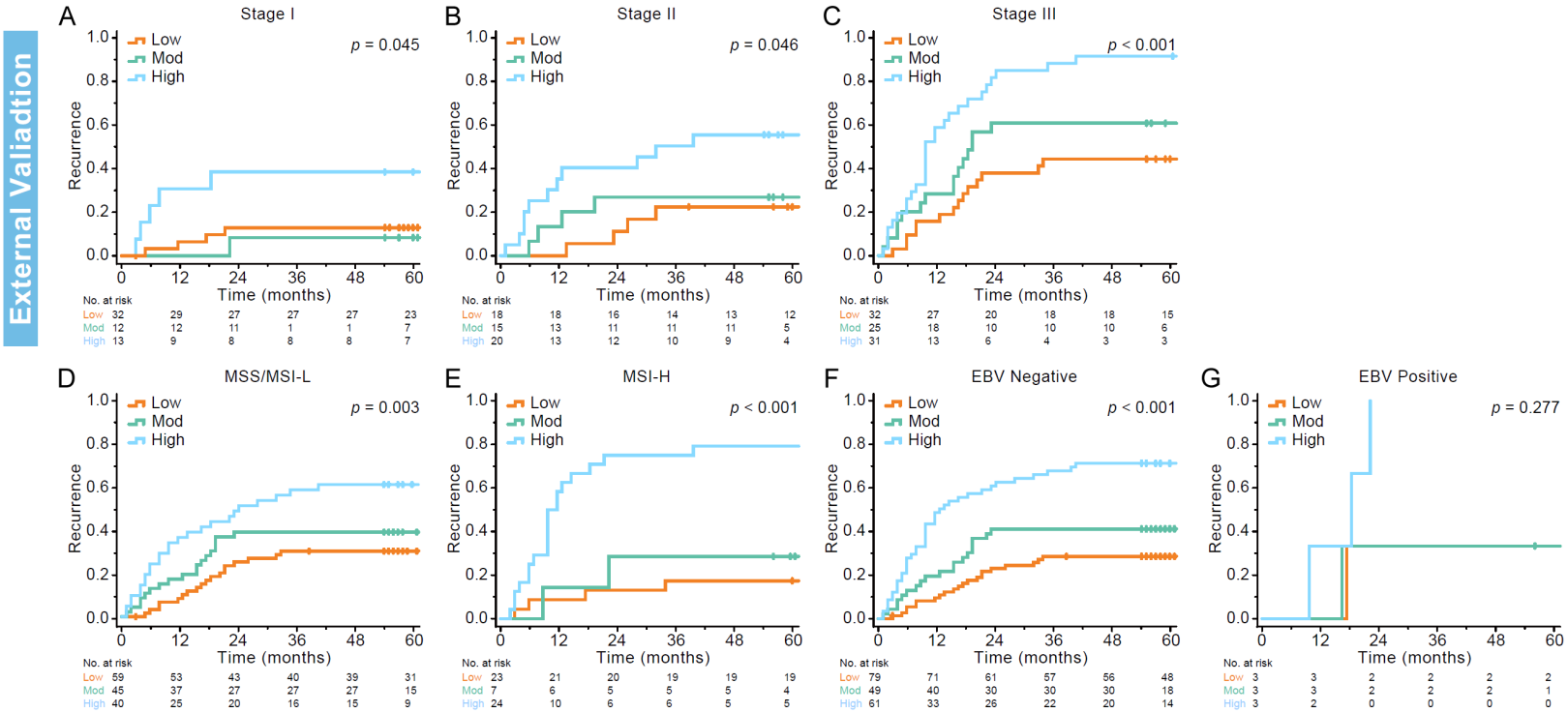

Figure S8. In the external validation cohort, stratified analysis showed that IRS was applicable to predict recurrence of postoperative GC patients with different clinicopathological characteristics. A-C. TNM stage. D, E. Microsatellite instability (MSI) status. F, G. Epstein-Barr virus (EBV) status. *P*-values were calculated using the log-rank test.

Table S2. Clinicopathological Characteristics of Patients with Gastric Cancer According to Immunosuppressive Recurrence Score Group in Internal Cohorts

Variable	Training Cohort (N=418)							Internal Validation Cohort (N=209)						
	Low Risk		Mod Risk		High Risk		*P**	Low Risk		Mod Risk		High Risk		*P**
	N	%	N	%	N	%		N	%	N	%	N	%	
Total patients	147	-	198	-	73	-		68	-	103	-	38	-	
Age (years)							0.646							0.802
≤65	93	63.3	131	66.2	44	60.3		40	58.8	60	58.3	20	52.6	
>65	54	36.7	67	33.8	29	39.7		28	41.2	43	41.7	18	47.4	
Sex							0.325							0.496
Female	33	22.4	52	26.3	13	17.8		16	23.5	28	27.2	13	34.2	
Male	114	77.6	146	73.7	60	82.2		52	76.5	75	72.8	25	65.8	
BMI							0.369							0.767
≤25	120	81.6	166	83.8	65	89.0		59	86.8	88	85.4	31	81.6	
>25	27	18.4	32	16.2	8	11.0		9	13.2	15	14.6	7	18.4	
Resection type							0.009							0.125
Part gastrectomy	76	51.7	85	42.9	22	30.1		38	55.9	45	43.7	14	36.8	
Total gastrectomy	71	48.3	113	57.1	51	69.9		30	44.1	58	56.3	24	63.2	
Tumor size							0.142							0.001
≤50 mm	56	38.1	86	43.4	38	52.1		49	72.1	48	46.6	15	39.5	
>50 mm	91	48.3	122	56.6	35	47.9		19	27.9	55	53.4	23	60.5	
Tumor location							0.006							0.129
Cardia	35	24.0	52	26.3	14	19.2		16	23.5	26	25.2	10	26.3	
Body	26	17.8	41	20.7	21	28.8		6	8.8	20	19.4	6	15.8	
Antrum	75	51.4	88	44.4	23	31.5		39	57.4	41	39.8	13	34.2	
Whole	10	6.8	17	8.6	15	20.5		7	10.3	16	15.5	9	23.7	
Grade							0.333							0.036
Low	63	42.9	93	47.0	33	45.2		30	44.1	52	50.5	23	60.5	
Middle + High	57	38.8	67	33.8	20	27.4		30	44.1	32	31.1	6	15.8	
Mix	20	13.6	29	14.6	18	24.7		8	11.8	118	17.5	7	18.4	
Unknow	7	4.8	9	4.5	2	2.7		0	0.0	1	1.0	2	5.3	
Depth of invasion							<0.001							0.002
T1	27	18.4	11	5.6	2	2.7		19	27.9	16	15.5	1	2.6	
T2	19	12.9	24	12.1	3	4.1		12	17.6	7	6.8	3	7.9	
T3	47	32.0	77	38.9	25	43.2		25	36.8	48	46.6	19	50.0	
T4	54	36.7	86	43.4	43	58.9		12	17.6	32	31.1	15	39.5	
Lymph node metastasis							<0.001							0.054
N0	5	3.4	3	1.5	0	0.0		31	45.6	33	32.0	7	18.4	
N1	68	46.3	74	37.4	19	26.0		13	19.1	21	20.4	6	15.8	
N2	36	24.5	47	23.7	7	9.6		10	14.7	13	2.6	9	23.7	
N3	38	25.9	74	37.4	47	64.4		14	20.6	36	35.0	16	42.1	
AJCC (7th)							0.003							<0.001
I	30	20.4	22	11.1	3	4.1		24	35.2	18	17.5	2	5.3	
II	39	26.5	58	29.3	16	21.9		22	32.4	33	32.0	9	23.7	
III	78	53.1	118	59.6	54	74.0		22	32.4	52	50.5	27	71.1	
MSI status							0.301							0.584
MSS/MSI-L	114	77.6	160	80.8	63	86.3		54	79.4	82	79.6	33	86.8	
MSI-H	33	22.4	38	19.2	10	13.7		14	20.6	21	20.4	5	13.2	
EBV status							0.087							0.529
Negative	143	97.3	184	92.9	66	90.4		68	94.1	95	92.2	37	97.4	

Positive	4	2.7	14	7.1	7	9.6		4	5.9	8	7.8	1	2.6	
Adjuvant chemotherapy							0.423							0.332
Yes	72	49.0	111	56.1	38	52.1		33	48.5	53	48.5	24	63.2	
No	75	51.0	87	43.9	35	47.9		35	51.5	50	51.5	14	36.8	
CEA							0.222							0.144
Normal	128	87.1	160	80.8	58	79.5		66	97.1	92	89.3	33	86.8	
Elevated	19	12.9	38	19.2	15	20.5		2	2.9	11	10.7	5	13.2	
CA19-9							0.044							0.032
Normal	125	85.0	153	77.3	52	71.2		61	89.7	78	75.7	27	71.1	
Elevated	22	15.0	45	22.7	21	28.8		7	10.3	25	24.3	11	28.9	

*Calculated by χ^2 test.

Table S3. Clinicopathological Characteristics of Patients with Gastric Cancer According to Immunosuppressive Recurrence Score Group in External Validation Cohort

Variable	External Validation Cohort (N=198)						*P**
	Low Risk		Mod Risk		High Risk		
	N	%	N	%	N	%	
Total patients	82	-	52	-	64	-	
Age (years)							0.849
≤65	59	72.0	35	67.3	46	71.9	
>65	23	28.0	17	32.7	18	28.1	
Sex							0.852
Female	23	28.0	17	32.7	20	31.3	
Male	59	72.0	35	67.3	44	68.8	
Resection type							0.406
Part gastrectomy	56	68.3	41	78.8	47	73.4	
Total gastrectomy	26	31.7	11	21.2	17	26.6	
Tumor size							0.540
≤50 mm	58	70.7	38	73.1	41	64.1	
>50 mm	24	29.3	14	26.9	23	35.9	
Grade							0.165
Low	29	35.4	15	28.8	23	35.9	
Middle + High	35	42.7	24	46.2	17	26.6	
Mix	16	19.5	13	25.0	23	35.9	
Unknow	2	2.4	0	0.0	1	1.6	
Depth of invasion							0.005
T1	22	26.8	8	15.4	6	9.4	
T2	16	19.5	10	19.2	15	23.4	
T3	2	2.4	10	19.2	5	7.8	
T4	42	51.2	24	46.2	38	59.4	
Lymph node metastasis							0.122
N0	44	53.7	25	48.1	25	39.1	
N1	17	20.7	9	17.3	8	12.5	
N2	12	14.6	6	11.5	13	20.3	
N3	9	11.0	12	23.1	18	28.1	
AJCC (7th)							0.118
I	32	39.0	12	23.1	13	20.3	
II	18	22.0	15	28.8	20	31.3	
III	32	39.0	25	48.1	31	48.4	

MSI status							0.015
MSS/MSI-L	59	72.0	45	86.5	40	62.5	
MSI-H	23	28.0	7	13.5	24	37.5	
EBV status							0.910
Negative	79	96.3	49	94.2	61	95.3	
Positive	3	3.7	3	5.8	3	4.7	
Adjuvant chemotherapy							0.763
Yes	44	53.7	25	48.1	31	48.4	
No	38	46.3	27	51.9	33	51.6	

*Calculated by χ^2 test.

Table S4. Univariate Analysis of Clinicopathological Characteristics Associated with Recurrence-Free Survival in the Training Cohort and Internal Validation Cohort

Variable	Training Cohort		Internal Validation Cohort	
	HR (95% CI)	*P*	HR (95% CI)	*P*
IRS	2.962 (2.420, 3.625)	<0.001	2.653 (2.026, 3.476)	<0.001
Age (≤65 vs >65)	1.119 (0.836, 1.499)	0.449	0.904 (0.601, 1.359)	0.628
Sex (Female vs Male)	0.862 (0.626, 1.187)	0.364	0.879 (0.562, 1.375)	0.573
BMI (≤25 vs >25)	0.878 (0.588, 1.311)	0.525	0.732 (0.390, 1.373)	0.331
Resection type (Part vs Total)	0.828 (0.622, 1.103)	0.197	3.144 (2.039, 4.846)	0.028
Tumor size (≤50 vs >50)	1.397 (1.053, 1.854)	0.020	1.397 (1.053, 1.854)	<0.001
Tumor location		0.039		0.076
Cardia	0.549 (0.335, 0.900)		0.660 (0.361, 1.205)	
Body	0.814 (0.502, 1.319)		0.724 (0.372, 1.408)	
Antrum	0.602 (0.387, 0.937)		0.481 (0.275, 0.841)	
Whole	Reference		Reference	
Grade		0.201		0.004
Low	0.867 (0.558, 1.347)		0.542 (0.132, 2.222)	
Middle + High	1.297 (0.616, 2.731)		0.213 (0.049, 0.919)	
Mix	1.217 (0.807, 1.833)		0.440 (0.101, 1.918)	
Unknow	Reference		Reference	
Depth of invasion		<0.001		<0.001
T1	0.225 (0.109, 0.461)		0.123 (0.049, 0.311)	
T2	0.214 (0.104, 0.439)		0.161 (0.058, 0.448)	
T3	0.705 (0.522, 0.954)		0.457 (0.298, 0.701)	
T4	Reference		Reference	
Lymph node metastasis		<0.001		<0.001
N0	0.199 (0.049, 0.807)		0.107 (0.054, 0.212)	
N1	0.202 (0.141, 0.289)		0.280 (0.152, 0.516)	
N2	0.324 (0.221, 0.476)		0.608 (0.359, 1.03)	
N3	Reference		Reference	
AJCC (7th)		<0.001		<0.001
Stage I	0.202 (0.106, 0.384)		0.732 (0.39, 1.373)	
Stage II	0.375 (0.257, 0.547)		0.629 (0.415, 0.951)	
Stage III	Reference		Reference	
MSI status (MSI-H vs MSS/MSI-L)	0.848 (0.588, 1.224)	0.379	1.384 (0.858, 2.231)	0.183
EBV status (Positive vs Negative)	1.350 (0.783, 2.326)	0.280	0.418 (0.132, 1.319)	0.137
Adjuvant Chemotherapy (Yes vs NO)	0.683 (0.490, 0.938)	0.039	0.668 (0.445, 1.002)	0.051
CEA (Normal vs Elevated)	1.506 (1.066, 2.126)	<0.001	2.153 (1.173, 3.951)	0.013
CA19-9 (Normal vs Elevated)	1.851 (1.348, 2.540)	0.020	1.417 (0.885, 2.269)	0.147

Table S5. Multivariate Analysis of Clinicopathological Characteristics Associated with Recurrence-Free Survival in the Training Cohort and Internal Validation Cohort

Variable	Training Cohort		Internal Validation Cohort	
	HR (95% CI)	*P*	HR (95% CI)	*P*
IRS	2.620 (2.132, 3.220)	<0.001	2.769 (1.990, 3.854)	<0.001
Resection type (Part vs Total)	-		1.479 (0.950, 2.303)	0.083
Tumor size (≤50 vs >50)	1.297 (0.970, 1.735)	0.079	0.907 (0.549, 1.499)	0.704
Tumor location		0.423		
Cardia	1.029 (0.616, 1.720)		-	
Body	1.348 (0.824, 2.204)		-	
Antrum	1.291 (0.819, 2.036)		-	
Whole	Reference		-	
Grade				0.258
Low	-		0.298 (0.068, 1.311)	
Middle + High	-		0.124 (0.027, 0.571)	
Mix	-		0.250 (0.054, 1.163)	
Unknow	-		Refernece	
Depth of invasion		0.003		0.017
T1	0.569 (0.262, 1.237)		0.383 (0.138, 1.060)	
T2	0.343 (0.161, 0.732)		0.299 (0.096, 0.928)	
T3	0.791 (0.578, 1.081)		0.521 (0.327, 0.830)	
T4	Reference		Reference	
Lymph node metastasis		<0.001		<0.001
N0	0.315 (0.076, 1.300)		0.126 (0.058, 0.271)	
N1	0.261 (0.175, 0.388)		0.376 (0.192, 0.735)	
N2	0.385 (0.259, 0.572)		0.614 (0.355, 1.060)	
N3	Reference		Reference	
Adjuvant Chemotherapy (Yes vs NO)	1.903 (1.410, 2.567)	<0.001	3.140 (1.996, 4.940)	<0.001
CEA (Normal vs Elevated)	0.780 (0.542, 1.123)	0.181	0.579 (0.301, 1.116)	0.103
CA19-9 (Normal vs Elevated)	0.658 (0.471, 0.921)	0.015	-	

Table S6. Univariate and Multivariate Analysis of Clinicopathological Characteristics Associated with Recurrence-Free Survival in the External Validation Cohort

Variable	Univariate Analyses		Multivariate Analyses	
	HR (95% CI)	*P*	HR (95% CI)	*P*
IRS	1.713 (1.400, 2.095)	<0.001	1.588 (1.285, 1.962)	<0.001
Age (≤65 vs >65)	1.041 (0.650, 1.668)	0.867	-	
Sex (Female vs Male)	0.843 (0.537, 1.324)	0.458	-	
Resection type (Part vs Total)	1.445 (0.920, 2.270)	0.110	-	
Tumor size (≤50 vs >50)	0.668 (0.432, 1.032)	0.069	-	
Grade		0.098		
Low	1.537 (0.902, 2.620)		-	
Middle + High	0.838 (0.474, 1.482)		-	
Mix	Reference		-	
Unknow	0 (0, 1.487E + 265)		-	
Depth of invasion		<0.001		0.018
T1	0.377 (0.193, 0.736)		0.565 (0.265, 1.202)	
T2	0.219 (0.100, 0.479)		0.280 (0.123, 0.635)	
T3	0.743 (0.356, 1.554)		0.782 (0.371, 1.650)	
T4	Reference		Reference	
Lymph node metastasis		<0.001		<0.001
N0	0.193 (0.112, 0.332)		0.278 (0.155, 0.500)	
N1	0.279 (0.142, 0.546)		0.360 (0.182, 0.714)	
N2	0.640 (0.363, 1.128)		0.619 (0.349, 1.099)	
N3	Reference		Reference	
AJCC (7th)		<0.001		
Stage I	0.197 (0.100, 0.387)		-	
Stage II	0.433 (0.257, 0.728)		-	
Stage III	Reference		-	
MSI status (MSI-H vs MSS/MSI-L)	1.162 (0.730, 1.852)	0.526	-	
EBV status (Positive vs Negative)	1.254 (0.508, 3.097)	0.623	-	
Adjuvant Chemotherapy (Yes vs NO)	1.620 (1.056, 2.484)	0.027	2.051 (1.299, 3.237)	0.002

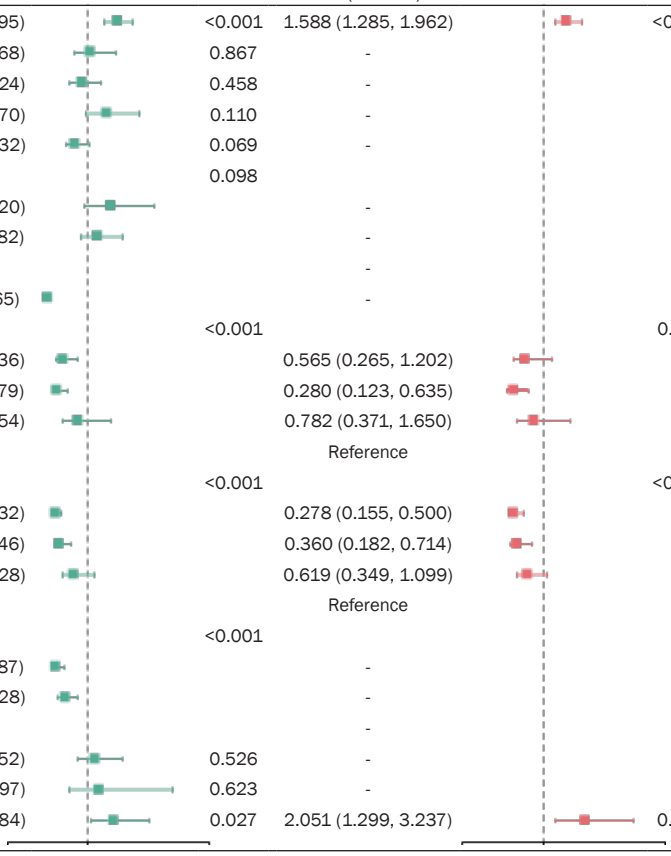

Immunosuppressive score to predict recurrence

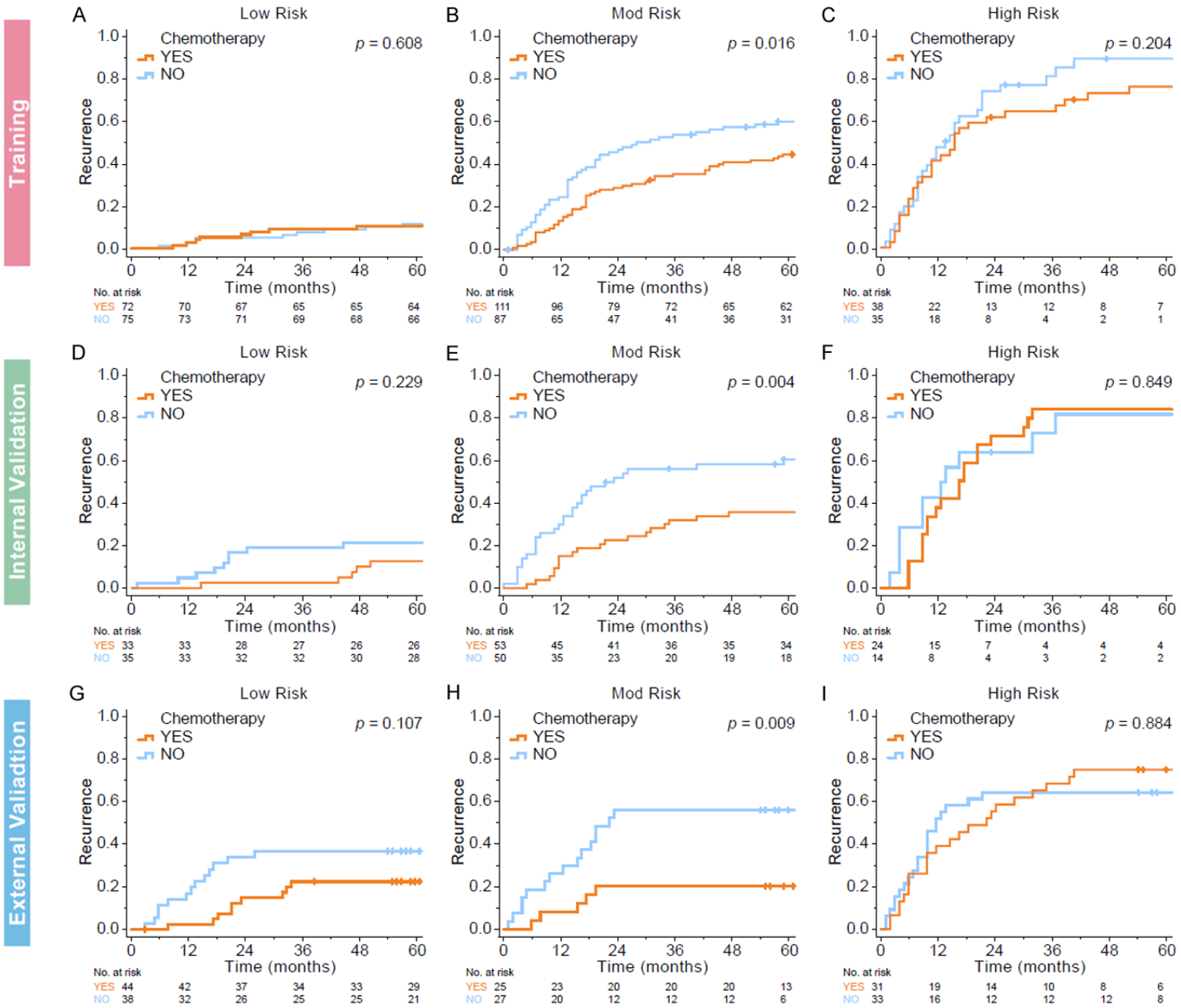

Figure S9. Patients in the moderated-risk group benefited from adjuvant chemotherapy after surgery, while those in the low-risk and high-risk groups did not. Kaplan-Meier curves of chemotherapy for recurrence-free survival (RFS). Training cohort: A. Low-risk group. B. Moderate-risk group. C. High-risk group. Internal validation cohort: D. Low-risk group. E. Moderate-risk group. F. High-risk group. External validation cohort: G. Low-risk group. H. Moderate-risk group. I. High-risk group. *P*-values of Kaplan-Meier curves were calculated using the log-rank test.

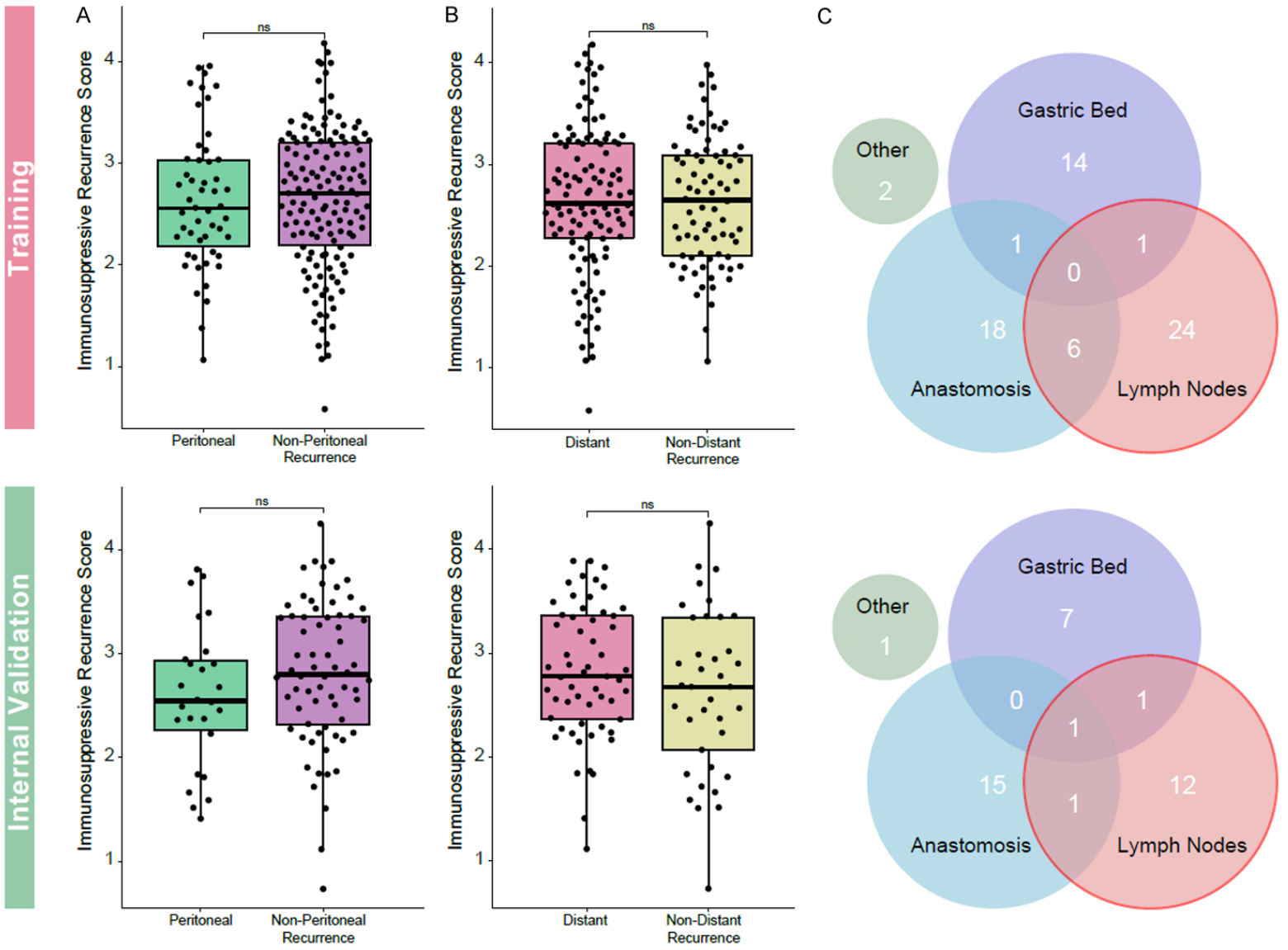

Figure S10. Peritoneal implants and distant metastasis were not associated with IRS. A. Comparison of IRS between patients with peritoneal implants and patients with non-peritoneal recurrence in the internal cohorts. B. Comparison of IRS between patients with distant metastasis and patients with non-distant recurrence in the internal cohorts. C. Venn diagram showing the recurrence site in patients with gastric cancer (GC) with locoregional recurrence from the internal cohorts. ns, not significant (Mann-Whitney U test).

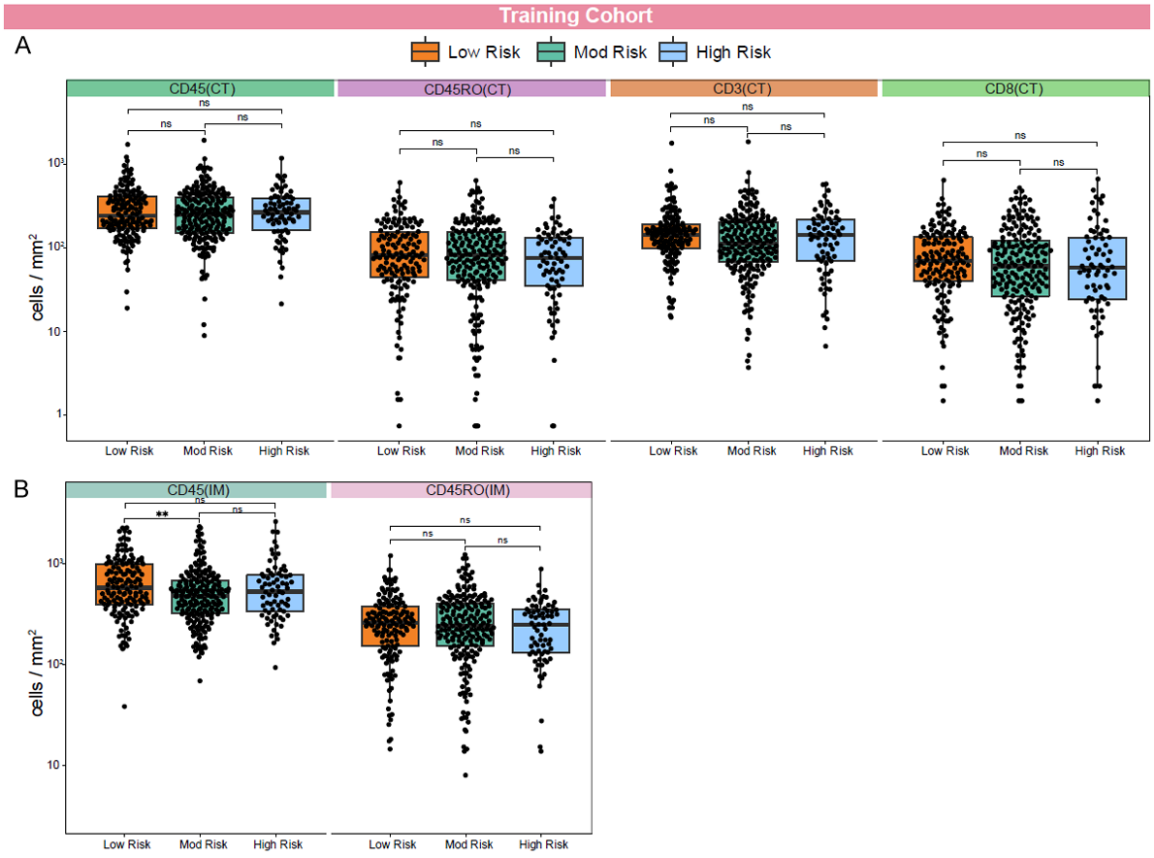

Figure S11. Association of immunosuppressive recurrence score (IRS) with the infiltration of immune biomarkers in the training cohort. A, B. Comparison of the expression of $CD45^{+}_{(CT)}$, $CD45RO^{+}_{(CT)}$, $CD3^{+}_{(CT)}$, $CD8^{+}_{(CT)}$, $CD45^{+}_{(IM)}$, and $CD45RO^{+}_{(IM)}$ in three subgroups (low-risk, moderate-risk, and high-risk subgroups) of patients with gastric cancer (GC). **P<0.01; ns, not significant (Kruskal-Wallis test).

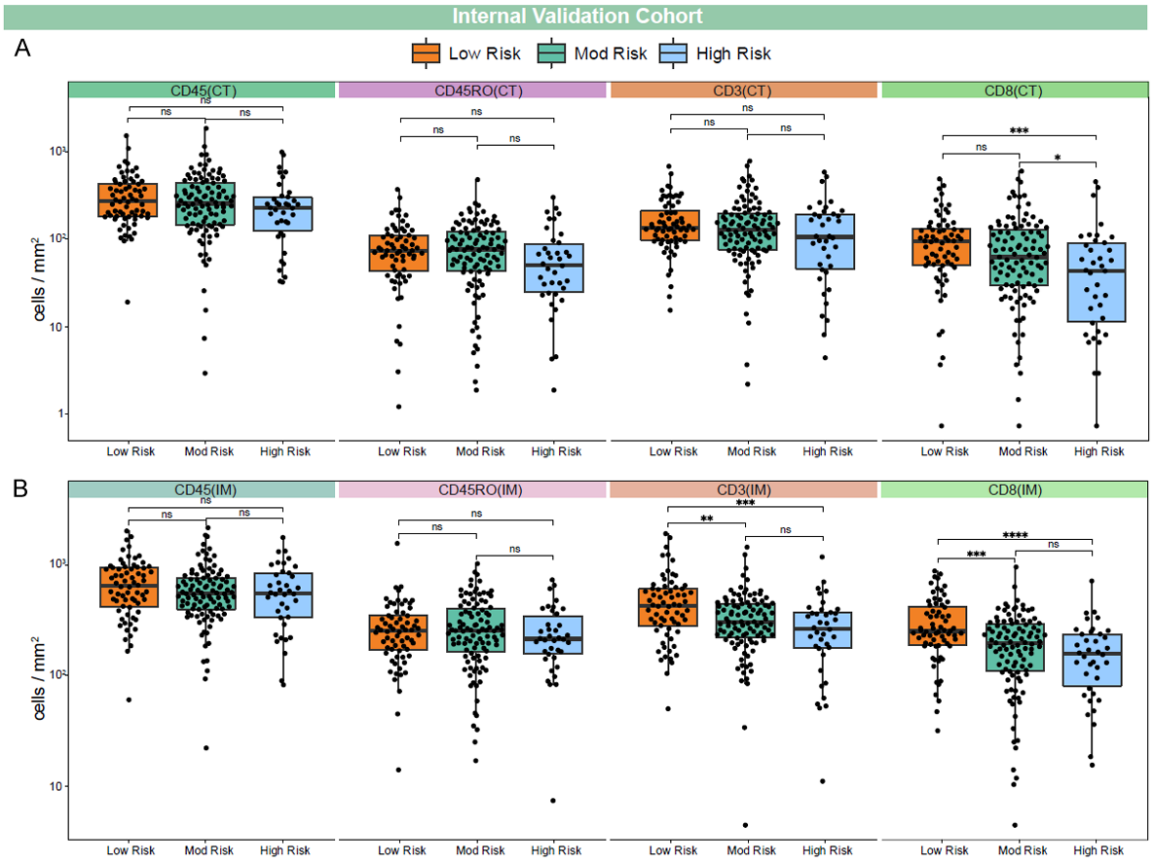

Figure S12. Association of immunosuppressive recurrence score (IRS) with the infiltration of immune biomarkers in the internal validation cohort. A, B. Comparison of the expression of $CD45^{+}_{(CT)}$, $CD45RO^{+}_{(CT)}$, $CD3^{+}_{(CT)}$, $CD8^{+}_{(CT)}$, $CD45^{+}_{(IM)}$, $CD45RO^{+}_{(IM)}$, $CD3^{+}_{(IM)}$, and $CD8^{+}_{(IM)}$ in three subgroups (low-risk, moderate-risk, and high-risk subgroups) of patients with gastric cancer (GC). *P<0.05; **P<0.01; ***P<0.001; ****P<0.0001; ns, not significant (Kruskal-Wallis test).

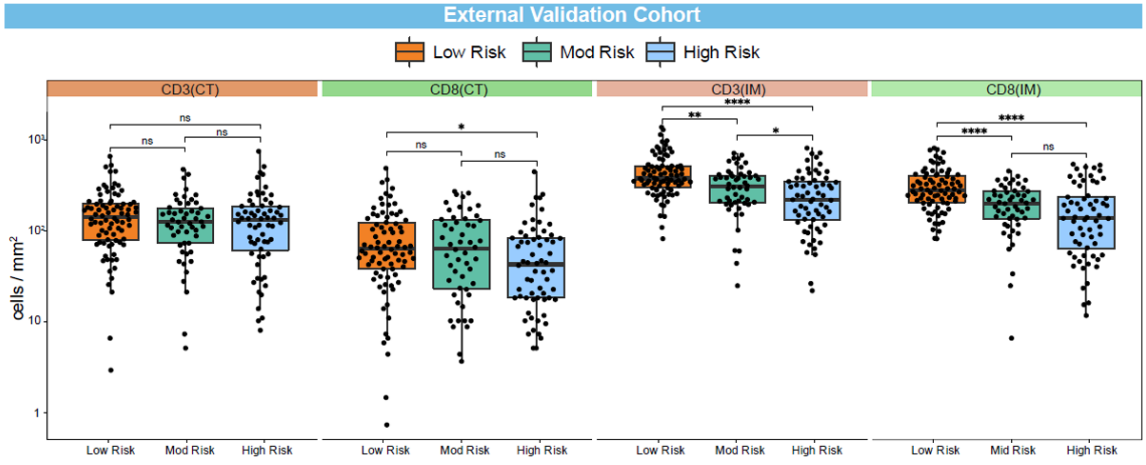

Figure S13. Association of immunosuppressive recurrence score (IRS) with the infiltration of immune biomarkers in the external validation cohort. Comparison of the expression of $CD3^{+}_{(CT)}$, $CD8^{+}_{(CT)}$, $CD3^{+}_{(IM)}$, and $CD8^{+}_{(IM)}$ in three subgroups (low-risk, moderate-risk, and high-risk subgroups) of patients with gastric cancer (GC). *P<0.05; **P<0.01; ****P<0.0001; ns, not significant (Kruskal-Wallis test).

Table S7. Clinicopathological Characteristics of Patients with Gastric Cancer for Multiplexed Immunofluorescence Staining According to Immunosuppressive Recurrence Score Group

Variable	Low Risk (N=15)		Mod Risk (N=15)		High Risk (N=15)		*P**
	N	%	N	%	N	%	
Age (years)							0.914
≤65	8	53.3	8	53.3	9	60.0	
>65	7	46.7	7	46.7	6	40.0	
Sex							0.678
Female	4	26.7	6	40.0	6	40.0	
Male	11	73.3	9	60.0	9	60.0	
BMI							0.887
≤25	11	73.3	12	80.0	11	73.3	
>25	4	26.7	3	20.0	4	26.7	
Resection type							0.529
Part gastrectomy	8	53.3	5	33.3	6	40.0	
Total gastrectomy	7	46.7	10	66.7	9	60.0	
Tumor size							0.144
≤50 mm	10	66.7	3	20.0	6	40.0	
>50 mm	5	33.3	12	80.0	9	60.0	
Tumor location							0.268
Cardia	5	33.3	5	33.3	2	13.3	
Body	2	13.3	5	33.3	4	26.7	
Antrum	8	53.3	4	26.7	6	40.0	
Whole	0	0.0	1	6.7	3	20.0	
Grade							0.528
Low	9	60.0	8	53.3	12	80.0	
Middle + High	4	26.7	4	26.7	1	6.7	
Mix	2	13.3	3	20.0	2	13.3	
Unknow	0	0.0	0	0.0	0	1.6	
Depth of invasion							0.053
T1	4	26.7	1	6.7	0	0.0	
T2	5	33.3	2	13.3	1	6.7	
T3	3	20.0	6	40.0	5	33.3	
T4	3	20.0	6	40.0	9	60.0	
Lymph node metastasis							0.091
N0	5	33.3	6	40.0	5	33.3	
N1	4	26.7	0	0.0	0	0.0	
N2	1	6.7	3	20.0	5	33.3	
N3	5	33.3	6	40.0	5	33.3	
AJCC (7th)							0.261
I	6	40.0	3	20.0	1	6.7	
II	3	20.0	3	20.0	3	20.0	
III	6	40.0	9	60.0	11	73.3	
MSI status							0.760
MSS/MSI-L	14	93.3	13	86.7	14	93.3	
MSI-H	1	6.7	2	13.3	1	6.7	
EBV status							0.844
Negative	12	80.0	13	86.7	13	86.7	
Positive	3	20.0	2	13.3	2	13.3	

Adjuvant chemotherapy							0.329
Yes	7	46.7	11	73.3	9	60.0	
No	8	53.3	4	26.7	6	40.0	
CEA							0.562
Normal	14	93.3	13	86.7	13	86.7	
Elevated	1	6.7	2	33.3	2	33.3	
CA19-9							0.544
Normal	13	86.7	11	73.3	13	86.7	
Elevated	2	13.3	4	26.7	2	13.3	

*Calculated by χ^2 test.

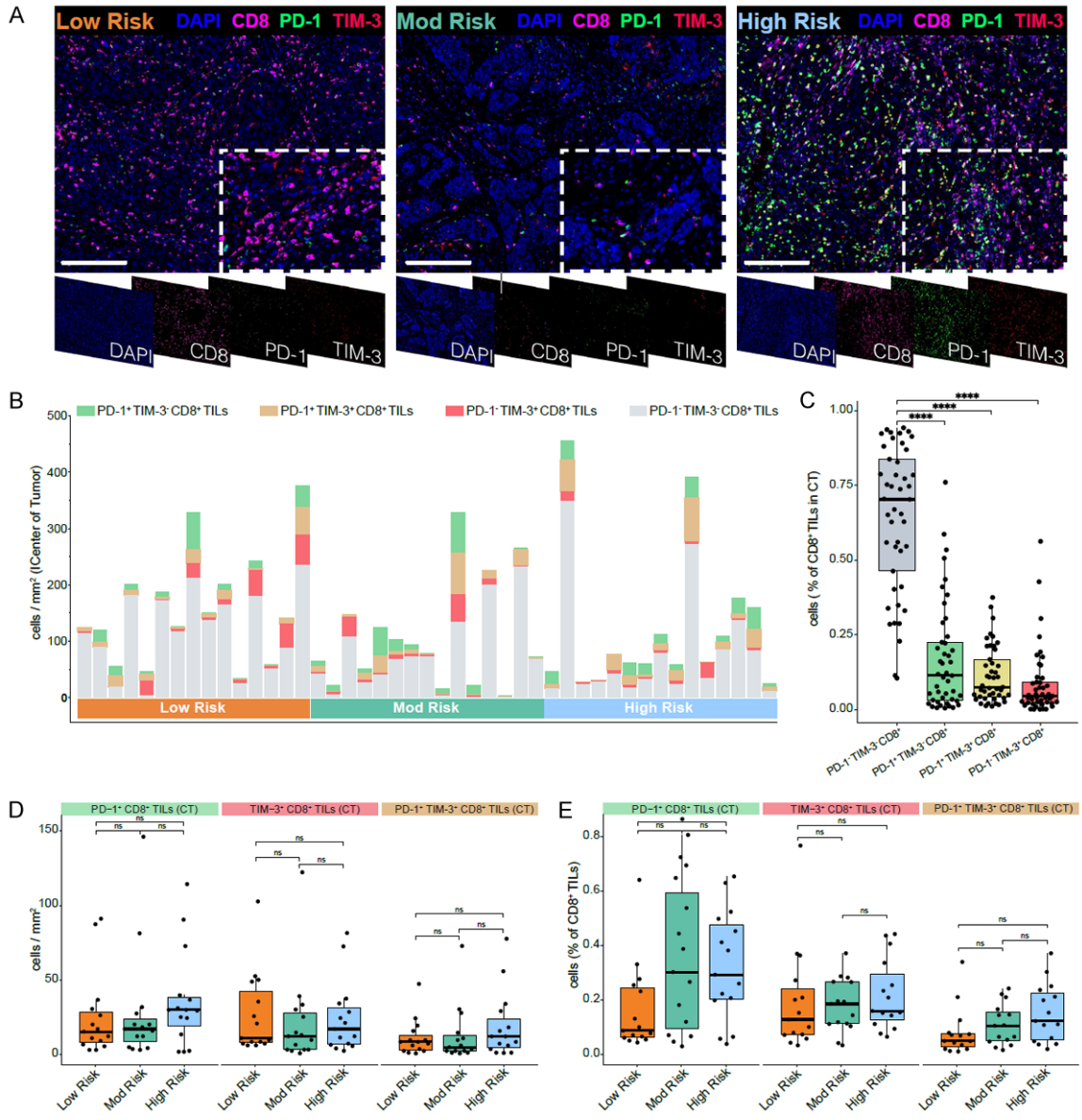

Figure S14. Multiplexed immunofluorescence (IF) staining reveals that there were no significant differences in immune checkpoint (PD-1 and TIM-3) expression among three groups in the center of tumor. A. Representative multiplexed IF images showing expression of PD-1 and TIM-3 in $CD8^{+}_{(CT)}$ T lymphocytes in the three risk subgroups of patients with gastric cancer (GC). B. In the low-risk (n=15), moderate-risk (n=15), and high-risk (n=15) groups, the different subtypes of $CD8^{+}_{(CT)}$ T lymphocytes were classified according to the expression of PD-1 and TIM-3. C.

Percentages of PD-1^{-}TIM-3^{-}CD8$^{+}_{(CT)}$, PD-1^{+}TIM-3^{-}CD8$^{+}_{(CT)}$, PD-1^{+}TIM-3^{+}CD8$^{+}_{(CT)}$ and PD-1^{-}TIM-3^{+}CD8$^{+}_{(CT)}$ T lymphocytes in 45 patients with GC. D. Comparison of the expression of PD-1^{+}CD8$^{+}_{(CT)}$, TIM-3^{+}CD8$^{+}_{(CT)}$, and PD-1^{+}TIM-3^{+}CD8$^{+}_{(CT)}$ in the low-risk (n=15), moderate-risk (n=15), and high-risk (n=15) groups of patients with GC. E. Comparison of the percentages of CD8^{+} lymphocytes expressing PD-1^{+}CD8$^{+}_{(CT)}$, TIM-3^{+}CD8$^{+}_{(CT)}$, and PD-1^{+}TIM-3^{+}CD8$^{+}_{(CT)}$ in the low-risk (n=15), moderate-risk (n=15), and high-risk (n=15) groups of patients with GC. *P<0.05; **P<0.01; ***P<0.001; ****P<0.0001 (Kruskal-Wallis test). Scale bar =200 μm.

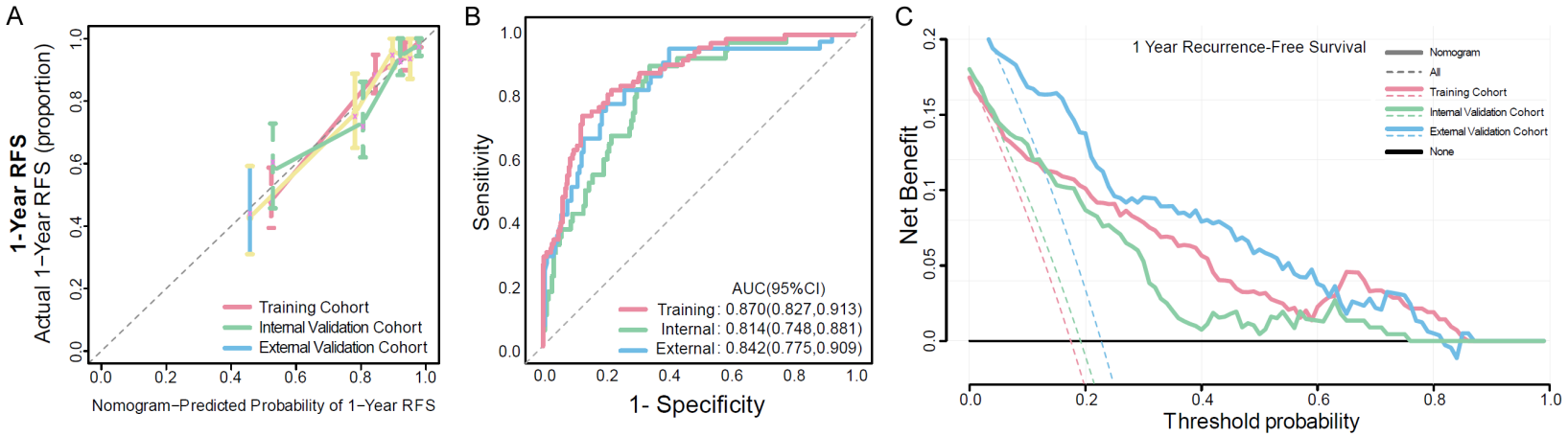

Figure S15. Validating the prognostic performance of a nomogram based on immunosuppressive recurrence score (IRS). A-C. Calibration curve, time-dependent receiver operator characteristic (ROC) curve, and decision curve analysis (DCA) for the nomogram in the training and internal and external validation cohorts.

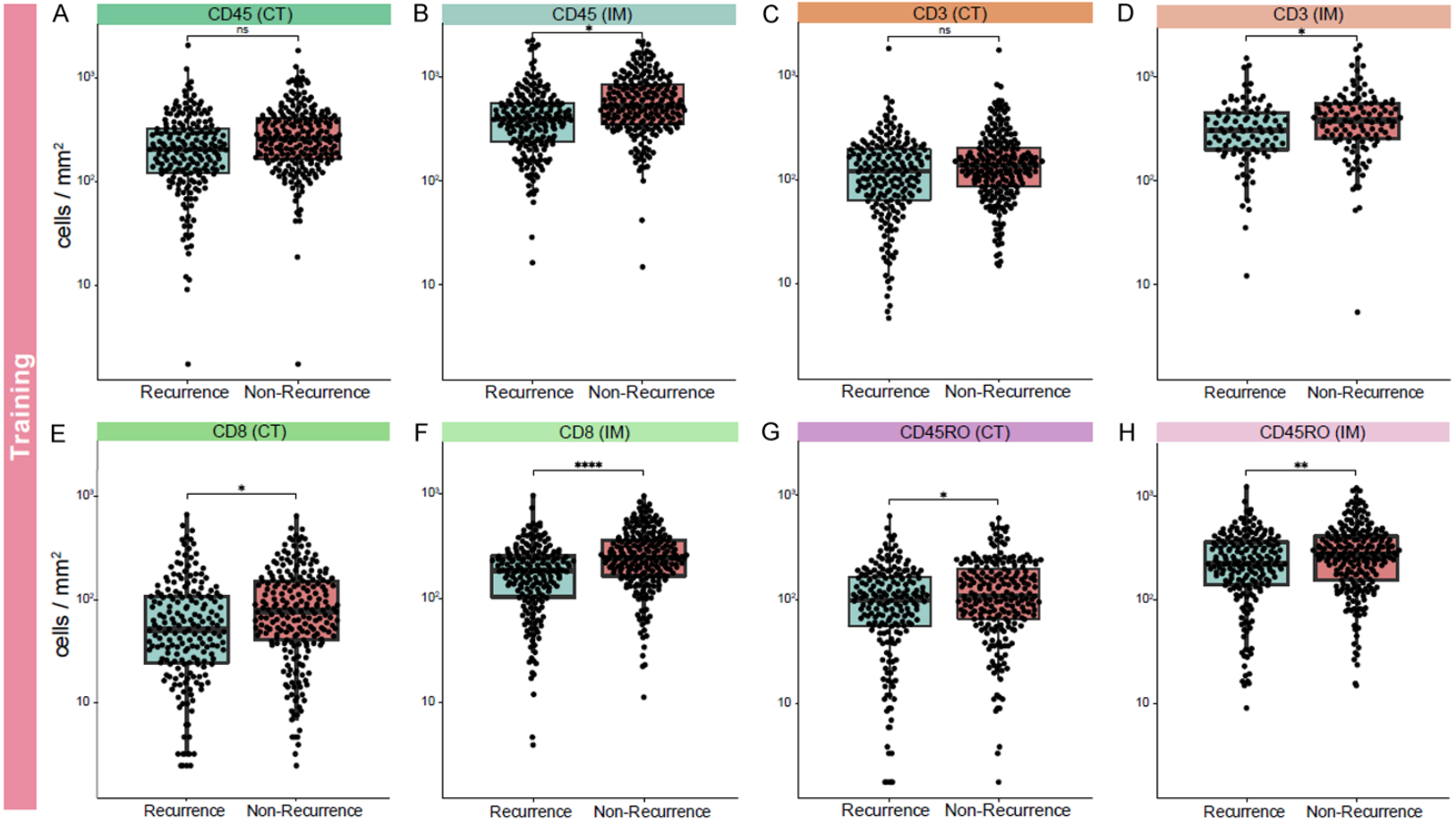
Training
A
CD45 (CT)
ns
B
CD45 (IM)
*
C
CD3 (CT)
ns
D
CD3 (IM)
*
E
CD8 (CT)
*
F
CD8 (IM)
****
G
CD45RO (CT)
*
H
CD45RO (IM)
**
cells / mm²
Recurrence
Non-Recurrence

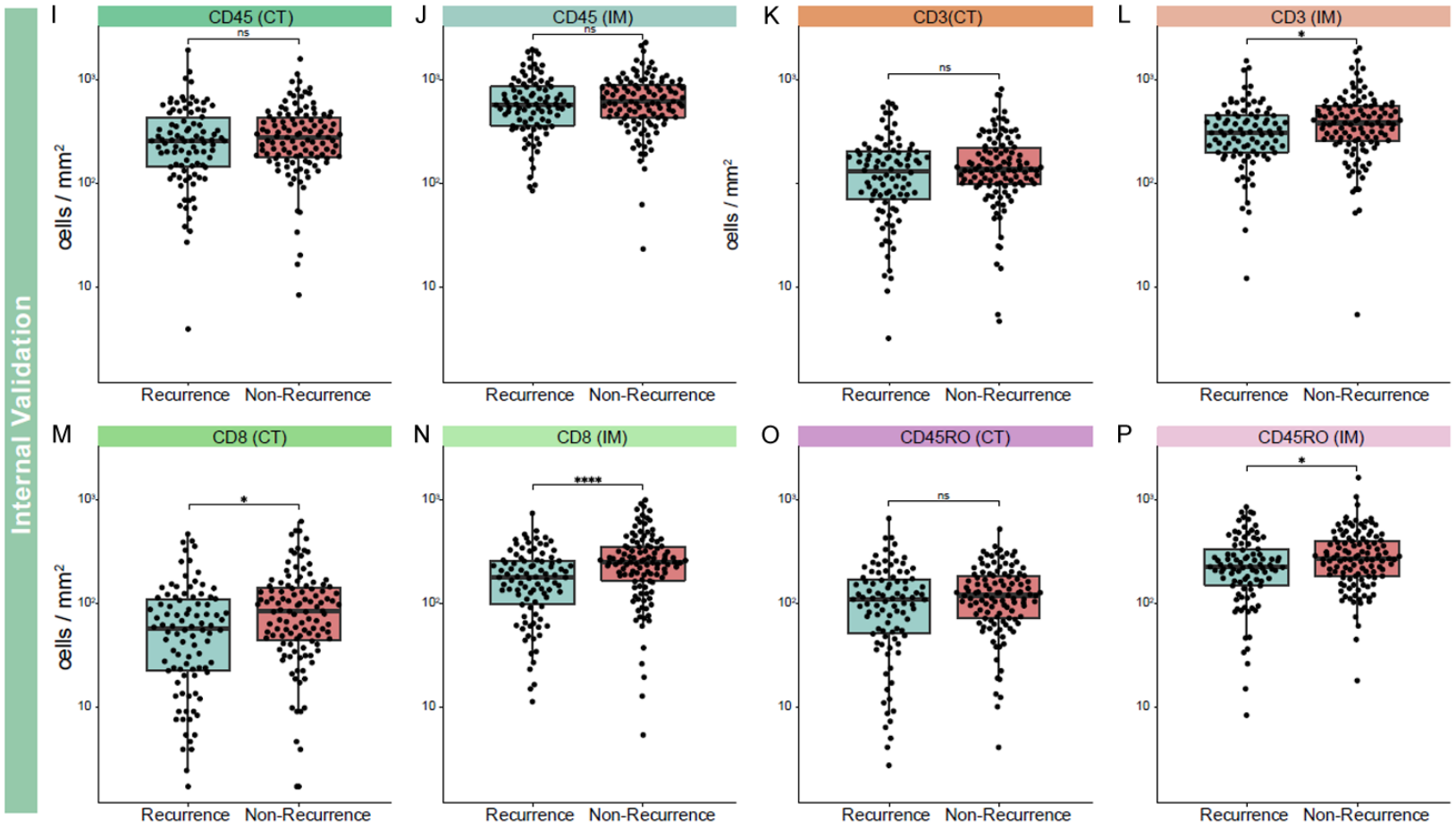
Internal Validation
I
CD45 (CT)
J
CD45 (IM)
K
CD3(CT)
L
CD3 (IM)
M
CD8 (CT)
N
CD8 (IM)
O
CD45RO (CT)
P
CD45RO (IM)
cells / mm²
ns
*
****
Recurrence
Non-Recurrence

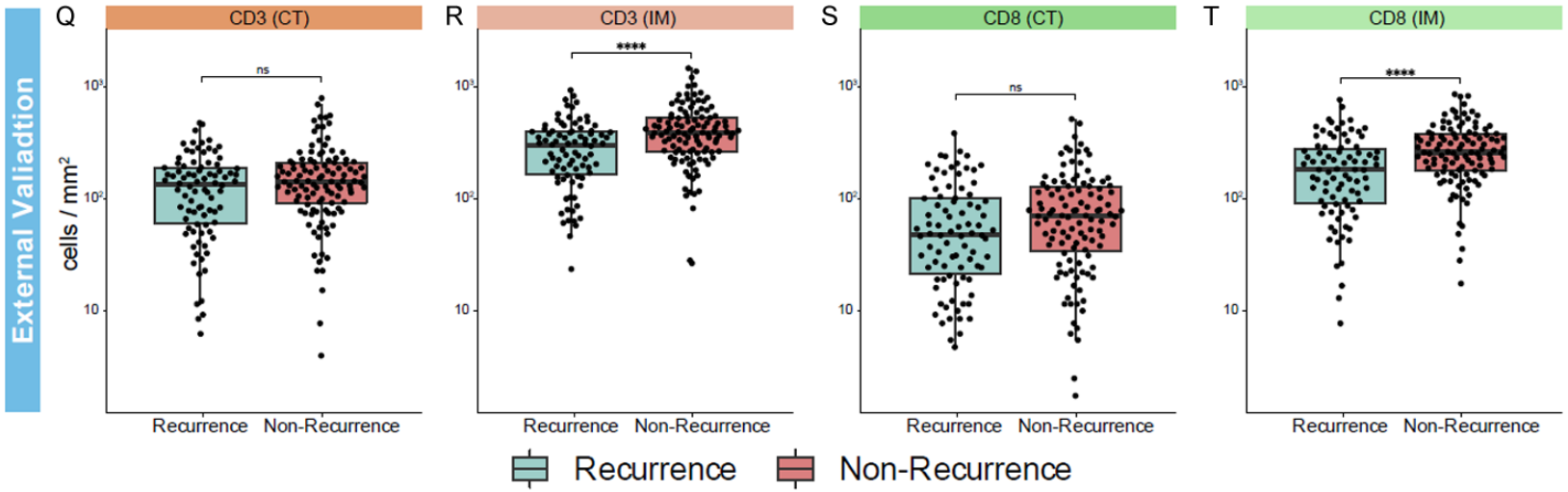

Figure S16. Comparison of the infiltration of immune cells between patients with gastric cancer (GC) with and without recurrence. A-H. Training cohort. I-P. Internal validation cohort. Q-T. External validation cohort. *P<0.05; **P<0.01; ****P<0.0001; ns, not significant (Mann-Whitney U test).